J. Fluid Mech. (2000), *vol.* 403, *pp.* 89–132. Printed in the United Kingdom

An explicit algebraic Reynolds stress model for incompressible and compressible turbulent flows

By STEFAN WALLIN[1] AND ARNE V. JOHANSSON[2]

[1]FFA, Box 11021, SE-161 11 Bromma, Sweden

[2]Department of Mechanics, KTH, SE-100 44 Stockholm, Sweden

(Received 6 November 1997 and in revised form 1 September 1999)

Some new developments of explicit algebraic Reynolds stress turbulence models (EARSM) are presented. The new developments include a new near-wall treatment ensuring realizability for the individual stress components, a formulation for compressible flows, and a suggestion for a possible approximation of diffusion terms in the anisotropy transport equation. Recent developments in this area are assessed and collected into a model for both incompressible and compressible three-dimensional wall-bounded turbulent flows. This model represents a solution of the implicit ARSM equations, where the production to dissipation ratio is obtained as a solution to a nonlinear algebraic relation. Three-dimensionality is fully accounted for in the mean flow description of the stress anisotropy. The resulting EARSM has been found to be well suited to integration to the wall and all individual Reynolds stresses can be well predicted by introducing wall damping functions derived from the van Driest damping function. The platform for the model consists of the transport equations for the kinetic energy and an auxiliary quantity. The proposed model can be used with any such platform, and examples are shown for two different choices of the auxiliary quantity.

1. Introduction

Standard two-equation models are still dominant in the context of industrial flow computations. In flows with strong effects of streamline curvature, adverse pressure gradients, flow separation or system rotation, such models fail to give accurate predictions. Turbulence models based on the transport equations for the individual Reynolds stresses have the natural potential for dealing with, for example, the associated complex dynamics of inter-component transfer. The Boussinesq hypothesis may in this context be said to be replaced by transport equations for the individual Reynolds stress anisotropies. As yet, there are non-trivial numerical aspects of flow computations with such models in complex flow situations. This represents an active area of research. In parallel with such efforts there has been a considerable renewed interest in various forms of algebraic approximations of the anisotropy transport equations. In the present work some new developments are presented for explicit formulations of algebraic Reynolds stress models. The motivation for this work is the general need for improvements in the prediction of complicated turbulent flows using the platform of existing CFD prediction tools based on the two-equation modelling level.

1.1. *Algebraic Reynolds stress models*

The classical algebraic Reynolds stress model (ARSM), Rodi (1972, 1976), was developed from the modelled Reynolds stress transport (RST) equation by assuming that the advection minus the diffusion of the individual Reynolds stresses can be expressed as the product of the corresponding quantity for the kinetic energy, K, and the individual Reynolds stresses normalized by K. This results in an implicit relation between the stress components and the mean velocity gradient field that replaces the Boussinesq hypothesis. Since the algebraic Reynolds stress model is determined from the modelled Reynolds stress transport equation no additional model constants are needed and the basic behaviour and experiences of the particular RST model will be inherited. The linearity of the Boussinesq hypothesis excludes any dependence on the rotational (antisymmetric) part of the mean velocity gradient tensor. An ARSM approach here represents a systematic method of constructing a nonlinear stress relationship that includes effects of the rotational part of the mean velocity gradient tensor. Despite this definite improvement one should, however, keep in mind that the ARSM can never represent the transport effects as well as a full RST model, which always should be expected to give a more correct description of the turbulence. However, the RST models also have limitations in predicting turbulence for general and complicated flows, especially in describing the effects of rotation.

The traditional ARSM idea is equivalent to neglecting advection and diffusion terms in the exact transport equation for the Reynolds stress anisotropy, a_{ij}, defined as $a_{ij} \equiv \overline{u_i u_j}/K - 2\delta_{ij}/3$. The advection term is indeed exactly zero for all stationary parallel mean flows, such as fully developed channel and pipe flows. For inhomogeneous flows the assumption of negligible effects of diffusion in the a_{ij} equation can cause problems, particularly in regions where the production term is small or where the inhomogeneity is strong. However, the Rodi ARSM assumption incorporates in a natural way not only effects of rotation but also effects of streamline curvature and three-dimensionality of the flow and has been found to be a reasonable approximation of the full differential RST equations in a number of flow situations, in many respects superior to the eddy-viscosity hypothesis.

To illustrate the natural way in which system rotation, and rotational effects in general, enter in this type of formalism we may take as the starting point the transport equation for the Reynolds stress anisotropy tensor in a rotating Cartesian coordinate system (the formulation of algebraic Reynolds stress models for rotating and curvilinear coordinate systems has recently been studied in some detail by Sjögren 1997)

$$K\frac{\mathrm{D}a_{ij}}{\mathrm{D}t} - \left(\frac{\partial T_{ijl}}{\partial x_l} - \frac{\overline{u_i u_j}}{K}\frac{\partial T_l^{(K)}}{\partial x_l}\right) = -\frac{\overline{u_i u_j}}{K}(\mathscr{P} - \varepsilon) + \mathscr{P}_{ij} - \varepsilon_{ij} + \Pi_{ij} + \varepsilon C_{ij}^{(a)}, \qquad (1.1)$$

where $-T_{ijl}$ and $-T_l^{(K)}$ are the fluxes (turbulent and molecular) of the Reynolds stress and turbulent kinetic energy, respectively. The dissipation rate tensor, ε_{ij}, and the pressure strain, Π_{ij}, need to be modelled whereas the production terms, $\mathscr{P}_{ij}$ and $\mathscr{P} = \mathscr{P}_{ii}/2$, and the Coriolis term, $C_{ij}^{(a)}$, do not need any modelling since they are explicit in the Reynolds stress tensor. In a non-rotating coordinate system the Reynolds stress production term is normally written as

$$\mathscr{P}_{ij} = -\overline{u_i u_k}U_{j,k} - \overline{u_j u_k}U_{i,k}, \qquad (1.2)$$

where $U_{i,j}$ denotes the mean velocity gradient tensor. In a rotating system it is

convenient to split the mean velocity gradient tensor into a mean strain and a mean rotation tensor. We will here let S_{ij} and Ω_{ij} denote these tensors normalized with the turbulent timescale, $\tau \equiv K/\varepsilon$,

$$S_{ij} = \frac{\tau}{2}\left(U_{i,j} + U_{j,i}\right), \quad \Omega_{ij} = \frac{\tau}{2}\left(U_{i,j} - U_{j,i}\right). \tag{1.3}$$

A consistent formulation of (1.1), valid also in the rotating system, can then be obtained by replacing the mean rotation tensor by the absolute rotation tensor

$$\Omega^*_{ij} = \Omega_{ij} + \Omega^{\mathrm{s}}_{ij}, \tag{1.4}$$

where

$$\Omega^{\mathrm{s}}_{ij} = \tau\epsilon_{jik}\omega^{\mathrm{s}}_k \tag{1.5}$$

and ω^{s}_k is the constant angular rotation rate vector of the system. This procedure illustrates the origin of the two parts of what normally is referred to as the Coriolis term in the a_{ij} equation. In this way the first part is included in the production term, that now (normalized with ε) can be expressed as

$$\frac{\mathscr{P}_{ij}}{\varepsilon} = -\tfrac{4}{3}S_{ij} - \left(a_{ik}S_{kj} + S_{ik}a_{kj}\right) + a_{ik}\Omega^*_{kj} - \Omega^*_{ik}a_{kj}. \tag{1.6}$$

The second part of the Coriolis term arises from the transformation of the advection term. This part (normalized by ε) is denoted by $C^{(a)}_{ij}$ in (1.1), and can be expressed as

$$C^{(a)}_{ij} = a_{ik}\Omega^{\mathrm{s}}_{kj} - \Omega^{\mathrm{s}}_{ik}a_{kj}. \tag{1.7}$$

The ARSM assumption results in the following implicit algebraic equation for a_{ij}:

$$\frac{\overline{u_iu_j}}{K}\left(\mathscr{P} - \varepsilon\right) = \mathscr{P}_{ij} - \varepsilon_{ij} + \Pi_{ij} + \varepsilon C^{(a)}_{ij}, \tag{1.8}$$

the structure of which, of course, depends on the choice of the models for ε_{ij} and Π_{ij}. For the present modelling purpose we choose an isotropic assumption for the dissipation rate tensor,

$$\varepsilon_{ij} = \tfrac{2}{3}\varepsilon\delta_{ij}, \tag{1.9}$$

and the Rotta model, Rotta (1951), for the slow pressure strain

$$\Pi^{(s)}_{ij} = -c_1\varepsilon a_{ij}. \tag{1.10}$$

For the rapid pressure–strain rate we choose the general linear model of Launder, Reece & Rodi (1975), which for a non-rotating system normally is written as

$$\Pi^{(r)}_{ij} = -\frac{c_2+8}{11}\left(\mathscr{P}_{ij} - \tfrac{2}{3}\mathscr{P}\delta_{ij}\right) - \frac{30c_2-2}{55}K\left(U_{i,j}+U_{j,i}\right) - \frac{8c_2-2}{11}\left(D_{ij} - \tfrac{2}{3}\mathscr{P}\delta_{ij}\right), \tag{1.11}$$

where $D_{ij} = -\overline{u_iu_k}U_{k,j} - \overline{u_ju_k}U_{k,i}$.

A simple way of obtaining a consistent, frame-independent formulation of the rapid pressure–strain rate model is to apply the same methodology as for the production term. This gives

$$\frac{\Pi^{(r)}_{ij}}{\varepsilon} = \tfrac{4}{5}S_{ij} + \frac{9c_2+6}{11}\left(a_{ik}S_{kj} + S_{ik}a_{kj} - \tfrac{2}{3}a_{km}S_{mk}\delta_{ij}\right) + \frac{7c_2-10}{11}\left(a_{ik}\Omega^*_{kj} - \Omega^*_{ik}a_{kj}\right). \tag{1.12}$$

From (1.8) we then obtain the implicit algebraic equation for the Reynolds stress anisotropy tensor in the form

$$\left(c_1 - 1 + \frac{\mathscr{P}}{\varepsilon}\right)\boldsymbol{a} = -\tfrac{8}{15}\boldsymbol{S} + \frac{7c_2+1}{11}(\boldsymbol{a\Omega}^{\mathrm{R}} - \boldsymbol{\Omega}^{\mathrm{R}}\boldsymbol{a}) - \frac{5-9c_2}{11}\left(\boldsymbol{aS} + \boldsymbol{Sa} - \tfrac{2}{3}\mathrm{tr}\{\boldsymbol{aS}\}\boldsymbol{I}\right). \tag{1.13}$$

In equation (1.13) $\boldsymbol{a}$, $\boldsymbol{S}$ and $\boldsymbol{\Omega}$ denote second-rank tensors, and $\boldsymbol{I}$ is the identity matrix. The inner product of two matrices is defined as $(\boldsymbol{SS})_{ij} \equiv \left(\boldsymbol{S}^2\right)_{ij} \equiv S_{ik}S_{kj}$ and tr{ } denotes the trace. This notation will be kept through this paper. One should note that (1.13) represents a nonlinear relation since $\mathscr{P}/\varepsilon \equiv -\mathrm{tr}\{\boldsymbol{aS}\}$.

It is interesting to note that the 'effective' mean rotation rate tensor, Ω_{ij}^{R}, depends on the choice of model:

$$\Omega_{ij}^{\mathrm{R}} = \Omega_{ij}^{*} + \frac{11}{7c_2+1}\Omega_{ij}^{\mathrm{s}} = \Omega_{ij} + \frac{7c_2+12}{7c_2+1}\Omega_{ij}^{\mathrm{s}}. \tag{1.14}$$

The ARSM approximation of the a_{ij} transport equation with this approach is then equivalent to neglecting the advective term (and diffusion) in the chosen rotating coordinate system. Hence, the adequacy of the ARSM approach is coupled to the choice of a coordinate system where the omission of advection terms in the a_{ij} equation can be justified. The choice of coordinate system is not at all trivial in strongly curved flows and the coordinate direction is not in general aligned with the flow direction. There are, however, methods to construct ARSMs that generally neglect only the advection term in the streamline direction (see e.g. Girimaji 1997 and Sjögren 1997).

As is seen from equation (1.13) the treatment of system rotation is quite straightforward. The superscript R on the mean rotation rate tensor will be dropped in the following.

The turbulent kinetic energy, $K \equiv \overline{u_i u_i}/2$, and its dissipation, ε, are determined from transport equations

$$\frac{\mathrm{D}K}{\mathrm{D}t} + \frac{\partial T_l^{(K)}}{\partial x_l} = \mathscr{P} - \varepsilon, \tag{1.15}$$

$$\frac{\mathrm{D}\varepsilon}{\mathrm{D}t} + \frac{\partial T_l^{(\varepsilon)}}{\partial x_l} = (C_{\varepsilon 1}\mathscr{P} - C_{\varepsilon 2}f_\varepsilon\varepsilon)\frac{\varepsilon}{K}. \tag{1.16}$$

There is no direct influence of system rotation on these equations. A substantial improvement over the eddy-viscosity model equations is that the production term, $\mathscr{P}$, does not need to be modelled. The transport terms, $T_l^{(K)}$ and $T_l^{(\varepsilon)}$, are usually modelled using gradient diffusion with the diffusivity coefficient expressed with the aid of the eddy viscosity, but here an improvement can also be achieved by using the knowledge of the complete Reynolds stress tensor. The gradient-diffusion model proposed by Daly & Harlow (1970) applied to the turbulent kinetic energy and its dissipation gives

$$T_l^{(K)} = -c_s'\frac{K}{\varepsilon}\overline{u_l u_m}\frac{\partial K}{\partial x_m}, \quad T_l^{(\varepsilon)} = -c_\varepsilon\frac{K}{\varepsilon}\overline{u_l u_m}\frac{\partial \varepsilon}{\partial x_m}. \tag{1.17}$$

Launder *et al.* (1975) recommend $c_s' = 0.25$ and $c_\varepsilon = 0.15$.

1.2. *Explicit algebraic Reynolds stress models*

The implicit relation for $\boldsymbol{a}$ in the ARSM equations has been found to be numerically and computationally cumbersome since there is no diffusion or damping present in

the equation system. In many applications the computational effort has been found to be excessively large and the benefits of using ARSM instead of the full Reynolds stress model are then lost. An explicit algebraic Reynolds stress model, EARSM, where the Reynolds stresses are explicitly related to the mean flow field is much more numerically robust and has been found to have almost a negligible effect on the computational effort as compared to a K–ε model.

The most general form for $\boldsymbol{a}$ in terms of $\boldsymbol{S}$ and $\boldsymbol{\Omega}$ consists of ten tensorially independent groups to which all higher-order tensor combinations can be reduced with the aid of the Caley–Hamilton theorem:

$$\begin{aligned}\boldsymbol{a} = {} & \beta_1\boldsymbol{S} + \beta_2\left(\boldsymbol{S}^2 - \tfrac{1}{3}II_S\,\boldsymbol{I}\right) + \beta_3\left(\boldsymbol{\Omega}^2 - \tfrac{1}{3}II_\Omega\,\boldsymbol{I}\right) + \beta_4\left(\boldsymbol{S}\boldsymbol{\Omega} - \boldsymbol{\Omega}\boldsymbol{S}\right)\\ & + \beta_5\left(\boldsymbol{S}^2\boldsymbol{\Omega} - \boldsymbol{\Omega}\boldsymbol{S}^2\right) + \beta_6\left(\boldsymbol{S}\boldsymbol{\Omega}^2 + \boldsymbol{\Omega}^2\boldsymbol{S} - \tfrac{2}{3}IV\,\boldsymbol{I}\right) + \beta_7\left(\boldsymbol{S}^2\boldsymbol{\Omega}^2 + \boldsymbol{\Omega}^2\boldsymbol{S}^2 - \tfrac{2}{3}V\,\boldsymbol{I}\right)\\ & + \beta_8\left(\boldsymbol{S}\boldsymbol{\Omega}\boldsymbol{S}^2 - \boldsymbol{S}^2\boldsymbol{\Omega}\boldsymbol{S}\right) + \beta_9\left(\boldsymbol{\Omega}\boldsymbol{S}\boldsymbol{\Omega}^2 - \boldsymbol{\Omega}^2\boldsymbol{S}\boldsymbol{\Omega}\right) + \beta_{10}\left(\boldsymbol{\Omega}\boldsymbol{S}^2\boldsymbol{\Omega}^2 - \boldsymbol{\Omega}^2\boldsymbol{S}^2\boldsymbol{\Omega}\right). \quad (1.18)\end{aligned}$$

The β-coefficients may be functions of the five independent invariants of $\boldsymbol{S}$ and $\boldsymbol{\Omega}$, which can be written as

$$II_S = \mathrm{tr}\{\boldsymbol{S}^2\}, \quad II_\Omega = \mathrm{tr}\{\boldsymbol{\Omega}^2\}, \quad III_S = \mathrm{tr}\{\boldsymbol{S}^3\}, \quad IV = \mathrm{tr}\{\boldsymbol{S}\boldsymbol{\Omega}^2\}, \quad V = \mathrm{tr}\{\boldsymbol{S}^2\boldsymbol{\Omega}^2\}. \quad (1.19)$$

Other scalar parameters may also be involved.

The independence of the ten groups and the completeness of expression (1.18) is further discussed in Appendix B. Shih & Lumley (1993) include also an eleventh, sixth-order group. The exact expression for such a group in terms of the lower-order groups is also given in Appendix B. In two-dimensional mean flows, there are only three independent tensor groups, i.e. the $\beta_{1,2,4}$ groups, and two independent invariants, II_S and II_Ω.

Formulation of expression (1.18) in terms of $\boldsymbol{S}$ and $\boldsymbol{\Omega}$ follows Pope (1975) and gives a much more compact form than by using the mean velocity gradients directly. It is also more cumbersome to compute matrix products involving $U_{i,j}$ due to the full matrix (eight independent elements) while S_{ij} and Ω_{ij} contain only five and three independent elements respectively. Also, the introduction of a rotating coordinate system is simplified here.

The main problem in obtaining an explicit relation for the anisotropy is that of determining the β-coefficients. A possibility would be to calibrate these from some chosen set of 'basic flows'. Shih, Zhu & Lumley (1992, 1995) partially adopted this approach combined with conditions related to realizability and restraints on correct behaviour in rapid distortion limits. A more traditional approach is to derive an explicit form from an implicit $\boldsymbol{a}$-relation based on established models for the terms in the Reynolds stress (or its anisotropy) tensor transport equation, equivalent to equation (1.13). Pope (1975) was the first to propose using the ten tensor groups to form a consistent explicit relation. He also derived a relation for two-dimensional mean flows leaving the production to dissipation ratio ($\mathscr{P}/\varepsilon$) implicit. This approach was later extended and solved for three-dimensional mean flows by Taulbee (1992) for the special case of $c_2 = \frac{5}{9}$ and by Gatski & Speziale (1993) for a general linear pressure–strain model.

The nonlinearity of equation (1.13) ($\mathscr{P}/\varepsilon \equiv -\mathrm{tr}\{\boldsymbol{a}\boldsymbol{S}\}$) forms a major obstacle for this approach and the studies published so far have circumvented the problem by letting $\mathscr{P}/\varepsilon = -\mathrm{tr}\{\boldsymbol{a}\boldsymbol{S}\}$ be implicit during the solution of (1.13), adopted by Pope

(1975) and Taulbee (1992) or the approach used by Gatski & Speziale (1993) where they used the asymptotic equilibrium value for $\mathscr{P}/\varepsilon$ as a universal constant.

The nonlinear system of equations is, however, conveniently solved in the form of a linear system of (five) equations complemented by a nonlinear scalar equation for $\mathscr{P}/\varepsilon$. For two-dimensional mean flows, Johansson & Wallin (1996) and Girimaji (1996*a*, *b*) have independently shown that this equation has a closed and fully explicit solution that can be expressed in a compact form. In the present work it is shown that good approximations are easily found for general three-dimensional mean flows. The complexity of the solution is substantially reduced by setting the coefficient $c_2 = \frac{5}{9}$ (see e.g. Taulbee 1992).

The removal of the need for *ad hoc* relations for $\mathscr{P}/\varepsilon$ represents a substantial improvement for this type of modelling. A constant $\mathscr{P}/\varepsilon$ gives wrong asymptotic behaviour for large strain rates, also noticed by Speziale & Xu (1996), while the fully consistent solution of the nonlinear equation system automatically fulfils the correct asymptotic behaviour. Also, in the very near-wall region, the correct asymptotic behaviour implies that all individual Reynolds stresses can be satisfactorily represented simply by introducing a van Driest damping function.

A straightforward extension to compressible flow is derived in which the mean density variations are taken into account. This model is applied to a complex flow situation with a shock–boundary layer interaction. An extension of the model to account in a simple way for the neglected turbulent transport of the anisotropies is also considered.

2. Formulation of an explicit algebraic model (EARSM)

The value of c_2 in the rapid pressure–strain model was originally suggested to be 0.4 by Launder *et al.* (1975), but more recent studies have suggested a higher value close to $\frac{5}{9}$, see e.g. Lumley (1978) and Shabbir & Shih (1992). This means that the last term in equation (1.13) is of quite small influence, also noticed by Taulbee (1992). Setting $c_2 = \frac{5}{9}$ one obtains the simplified but still implicit equation

$$\left(c_1 - 1 + \frac{\mathscr{P}}{\varepsilon}\right)\boldsymbol{a} = -\tfrac{8}{15}\boldsymbol{S} + \tfrac{4}{9}(\boldsymbol{a\Omega} - \boldsymbol{\Omega a}). \tag{2.1}$$

System rotation can easily be accounted for by substituting $\boldsymbol{\Omega}$ with $\boldsymbol{\Omega}^{\mathrm{R}} = \boldsymbol{\Omega} + (13/4)\boldsymbol{\Omega}^{\mathrm{s}}$ according to (1.14) where $\boldsymbol{\Omega}^{\mathrm{s}}$ is given by (1.5) (see § 1). It will be shown later that the removal of the last term in equation (1.13) gives a substantial simplification of the solution, especially in three-dimensional mean flow. The Rotta coefficient, c_1, is here set to 1.8.

The simplified but implicit algebraic Reynolds stress equation (2.1) is rewritten in the following form:

$$N\boldsymbol{a} = -\tfrac{6}{5}\boldsymbol{S} + (\boldsymbol{a\Omega} - \boldsymbol{\Omega a}), \tag{2.2}$$

where N is closely related to the production to dissipation ratio ($\mathscr{P}/\varepsilon = -\mathrm{tr}\{\boldsymbol{aS}\}$),

$$N = c_1' + \tfrac{9}{4}\mathscr{P}/\varepsilon \tag{2.3}$$

and

$$c_1' = \tfrac{9}{4}(c_1 - 1). \tag{2.4}$$

The procedure to solve this equation is the following: First, the general form for the anisotropy, equation (1.18), is inserted into the simplified ARSM equation (2.2) where

N is not yet determined. The resulting linear equation system for the β-coefficients is then solved by using the fact that higher-order tensor groups can be reduced with the aid of the Cayley–Hamilton theorem where the ten groups in the general form (1.18) form a complete basis. The β-coefficients are now functions of the production to dissipation ratio, $\mathscr{P}/\varepsilon$, or N. The final step is to formulate and solve the nonlinear scalar equation for N or $\mathscr{P}/\varepsilon$.

2.1. *Solution of the simplified ARSM for two-dimensional mean flows*

For two-dimensional mean flows the solution is reduced to only two non-zero coefficients, which can be expressed as

$$\beta_1 = -\frac{6}{5}\frac{N}{N^2 - 2II_\Omega}, \quad \beta_4 = -\frac{6}{5}\frac{1}{N^2 - 2II_\Omega}. \tag{2.5}$$

It is clearly seen that the denominator, $N^2 - 2II_\Omega$, cannot become singular since II_Ω is always negative. It will be shown later that an explicit formulation of any quasi-linear ARSM is non-singular if the corresponding nonlinear equation for the production to dissipation ratio is solved, as also noticed by Girimaji (1996*a*, *b*).

The nonlinear equation for N in two-dimensional mean flow can be derived by introducing the solution of $\boldsymbol{a}$ for two-dimensional mean flow in the definition of N. The resulting equation is cubic

$$N^3 - c_1' N^2 - \left(\tfrac{27}{10} II_S + 2II_\Omega\right) N + 2c_1' II_\Omega = 0, \tag{2.6}$$

and can be solved in a closed form with the solution for the positive root being

$$N = \begin{cases} \dfrac{c_1'}{3} + (P_1 + \sqrt{P_2})^{1/3} + \operatorname{sign}(P_1 - \sqrt{P_2}) \mid P_1 - \sqrt{P_2} \mid^{1/3}, & P_2 \geqslant 0 \\ \dfrac{c_1'}{3} + 2\left(P_1^2 - P_2\right)^{1/6} \cos\left(\dfrac{1}{3}\arccos\left(\dfrac{P_1}{\sqrt{P_1^2 - P_2}}\right)\right), & P_2 < 0 \end{cases} \tag{2.7}$$

where the arccos function should return an angle between 0 and π and

$$P_1 = (\tfrac{1}{27}c_1'^2 + \tfrac{9}{20}II_S - \tfrac{2}{3}II_\Omega)c_1', \quad P_2 = P_1^2 - (\tfrac{1}{9}c_1'^2 + \tfrac{9}{10}II_S + \tfrac{2}{3}II_\Omega)^3. \tag{2.8}$$

It can easily be shown that N remains real and positive for all possible values of II_S and II_Ω. The production to dissipation ratio may then be found from (2.3).

The above solution for two-dimensional flows was also given in Johansson & Wallin (1996) and is very similar in structure to that of Girimaji (1996*a*, *b*) who also derives an explicit solution for $\mathscr{P}/\varepsilon$ although for a somewhat more general set of models that yields $\beta_2 \neq 0$ (cf. the solutions in Appendix C).

2.1.1. *Illustration of the behaviour of the proposed model*

Figures 1 and 2 illustrate the behaviour of the solution for $\mathscr{P}/\varepsilon$. We note that it is zero for all cases with $\sigma = 0$, i.e. irrespective of the value of ω, where σ and ω are defined as $\sigma \equiv \sqrt{II_S/2}$ and $\omega \equiv \sqrt{-II_\Omega/2}$ and that the $\mathscr{P}/\varepsilon$ ratio decreases monotonically with increasing influence of rotation. For all parallel shear flows $\sigma = \omega$.

Homogeneous shear flow is a classical corner stone case for calibration of turbulence models. Tavoularis & Corrsin (1981) have experimentally shown that the asymptotic value of $SK/\varepsilon \approx 6$ corresponding to $\sigma = \omega = 3$. In the experiments the production to dissipation ratio was found to be approximately 1.8, marked as a circle in figure 2. The present model exactly replicates that result. Furthermore, in the log-layer of a boundary layer we know that the production balances the dissipation rate, $\mathscr{P} = \varepsilon$,

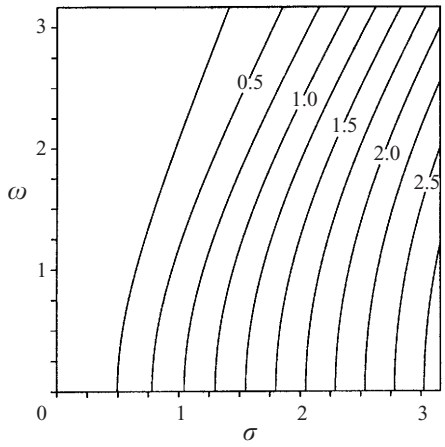

FIGURE 1. Isolines of the production to dissipation ratio for the current model.

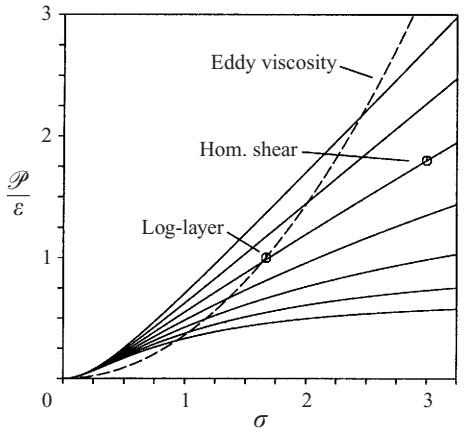

FIGURE 2. Production to dissipation ratio versus strain rate σ for different rotation ratios ω/σ. The current model (——) compared to an eddy-viscosity model (– – –).

which is obtained with the proposed model when the strain rate $\sigma = 1.69$. This is within the range of σ values found in the log-layer of the DNS data for channel flow (Kim 1989). This is also consistent with an effective $C_\mu = 0.09$ which gives $\sigma = 1.67$, also marked as a circle in the figure.

The anisotropies for the two cases are compared in tables 1 and 2. Most important is to correctly predict the a_{12} anisotropy since this is the only component of the anisotropy tensor that contributes to the turbulent production in parallel flows. The a_{22} component is also important since this is the only term that contributes to the turbulent diffusion term. The table shows that a_{12} and a_{22} are well predicted for the two different cases. The a_{11} and a_{33} components are, however, not as well predicted due to the simplification of setting $c_2 = \frac{5}{9}$ since this implies that $a_{33} = 0$. The inclusion of $c_2 \neq \frac{5}{9}$ will, however, not be sufficient if one wishes to improve the prediction of the anisotropies, since the particular choice of c_1 and c_2 used here is the only combination that predicts both a_{12} and a_{22} correctly in these two different cases. The good behaviour of the model for these two very different cases justifies the particular choice of model constants, c_1 and c_2, in the pressure–strain model.

	a_{12}	a_{11}	a_{22}	a_{33}	σ
DNS	−0.29	0.34	−0.26	−0.08	1.65
Current model	−0.30	0.25	−0.25	0.00	1.69

TABLE 1. The computed anisotropy in the log-layer using the current model assuming balance between turbulence production and dissipation compared to channel DNS data (Kim 1989).

	a_{12}	a_{11}	a_{22}	a_{33}	$\mathscr{P}/\varepsilon$
Experiment	−0.30	0.40	−0.28	−0.12	1.8
Current model	−0.30	0.31	−0.31	0.00	1.8

TABLE 2. The anisotropy in asymptotic homogeneous shear flow using the current model with $\sigma = 3.0$ compared to measurements by Tavoularis & Corrsin (1981).

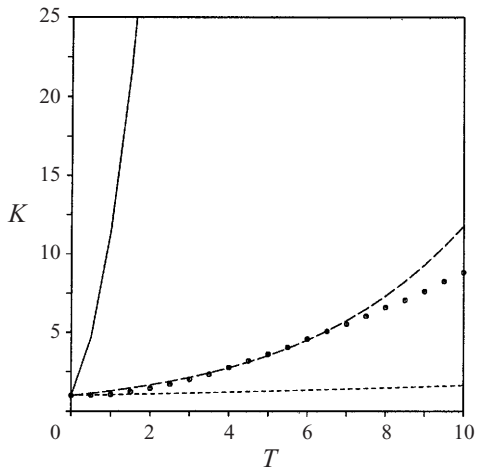

FIGURE 3. Time evolution of the turbulent kinetic energy in rapidly sheared homogeneous flow, $SK/\varepsilon = 50$. Eddy-viscosity model (——), the proposed EARSM (– – –) and the Gatski & Speziale (1993) EARSM (·····) compared with RDT (•).

A better tuning of the different anisotropies could possibly be achieved by using the most general quasi-linear pressure–strain model, where the coefficients may be functions of the production to dissipation ratio. This will be further discussed in § 2.3.

The asymptotic behaviour for large strain rates in parallel flow can be investigated by letting $\sigma = \omega \to \infty$. The production to dissipation ratio then becomes $\mathscr{P}/\varepsilon \sim \sigma$ and $\beta_1 \sim 1/\sigma$. This asymptotic behaviour for the β_1-coefficient (equivalent to $-2C_\mu$) is of particular interest since it ensures good model behaviour in the very near-wall buffer- and viscous sub-layers as will be shown later. The asymptotic behaviour is also consistent with the asymptotic characteristics of homogeneous shear flow. With an erroneous model assumption of a constant production to dissipation ratio, $\mathscr{P}/\varepsilon$, the wrong asymptote, $\beta_1 \sim 1/\sigma^2$, is obtained, as also noticed by Speziale & Xu (1996), while the solution of the nonlinear equation for $\mathscr{P}/\varepsilon$ automatically gives the correct asymptotic behaviour.

To illustrate the behaviour for large shear rates the model is tested in homogeneous shear flow at high initial shear rate ($SK/\varepsilon = 50$), see figure 3. This flow is a case where one should expect differences between the algebraic approach and the full

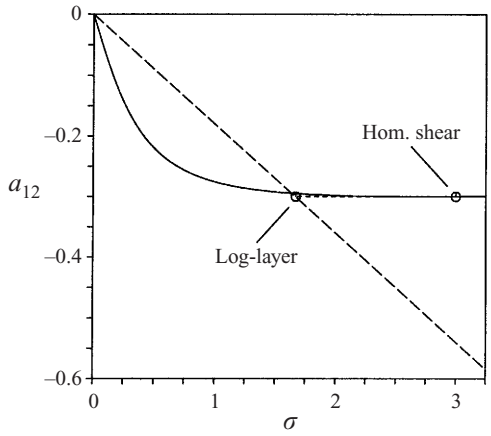

FIGURE 4. Predicted a_{12} anisotropy versus strain rate σ for parallel flow. The current model (——) compared to the eddy-viscosity model (– – –) and the Menter (1993) SST model (·····).

differential model due to the fact that the anisotropies undergo a temporal evolution ($\partial a_{ij}/\partial t \neq 0$) in the development towards an asymptotic state. Moreover, the Launder *et al.* (1975) model gives quite poor predictions of this case when used in a differential form. The very good predictions of the present EARSM can thus be regarded as a bit fortuitous. Nevertheless, the self-consistent approach gives a model with the correct asymptotic behaviour, which is a pre-requisite for reasonable predictions in the limit of high shear. It is important to make clear that the proposed model is not intended for these extreme high shear rates and the normal stress components are not as well predicted as the turbulent kinetic energy. It is, however, an important step towards a more general engineering model that the model is able to give reasonable results in extreme flow cases also.

In flows with an adverse pressure gradient, the production to dissipation ratio is greater than 1 and eddy-viscosity models with constant C_μ overestimate the turbulent viscosity or the a_{12} anisotropy. Bradshaw's assumption, which is adopted by Menter (1993) in the shear stress transport (SST) model, forces the a_{12} anisotropy to be constant for $\mathscr{P}/\varepsilon$ ratios greater than unity, which gives $\beta_1 \sim 1/\sigma$. This is fulfilled in the limit of large strain rates by the proposed model, which also gives a nearly constant a_{12} anisotropy in boundary layers with small pressure gradients. This can be seen in figure 4 where the a_{12} anisotropy versus the strain rate is shown for parallel flows. The a_{12} anisotropy computed from the proposed model is nearly constant here for a wide range of strain rates including both the log-layer and asymptotic homogeneous shear. The eddy-viscosity assumption gives $a_{12} = -2C_\mu\sigma$ and has a totally different behaviour, shown in the figure, and becomes physically unrealizable for large strain rates, $\sigma > 5.56$. This is, however, avoided by the SST limitation on the anisotropy which nearly coincides with the proposed model for strain rates larger than those in the log-layer. This feature of the proposed model ensures an improved behaviour in boundary layers with pressure gradients as compared to standard eddy-viscosity models.

Since equation (1.18) represents the general form of the anisotropy, different explicit algebraic Reynolds stress models can be compared by studying the behaviour of the β-coefficients. In two-dimensional mean flows the β-coefficients can be illustrated as iso-curves in the (σ, ω)-plane. In figure 5 the β_1-coefficient (equivalent to $-2C_\mu$) is

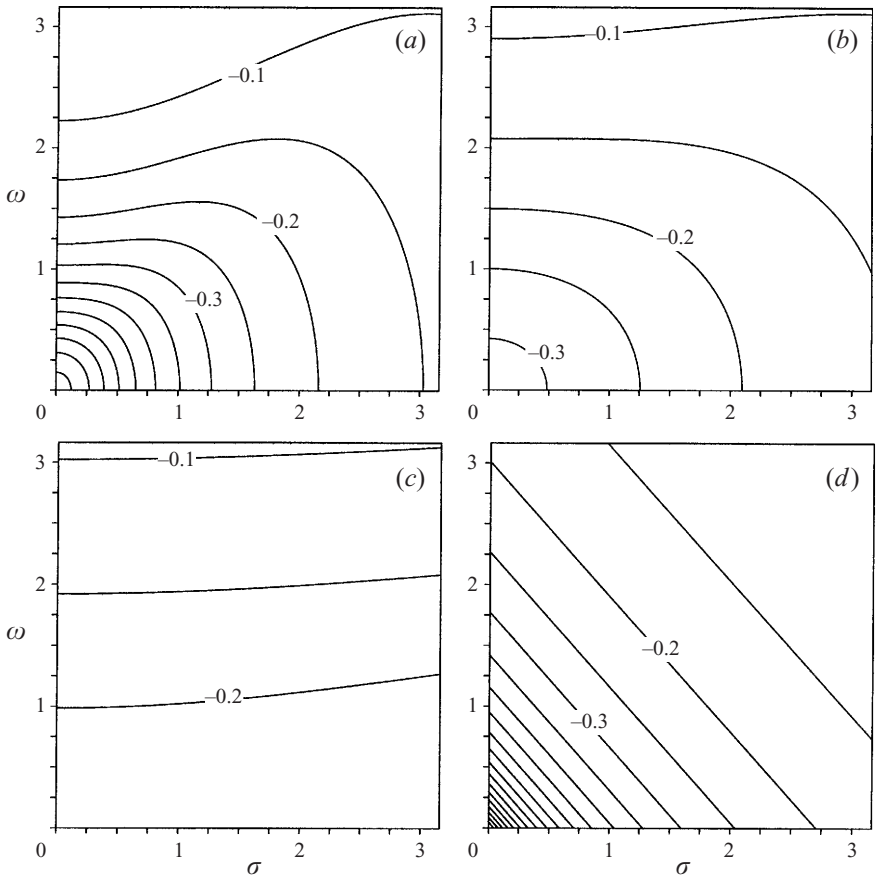

FIGURE 5. The behaviour of the β_1-coefficient in the (σ, ω)-plane for: (*a*) the implicit ARSM and the present EARSM, (*b*) Taulbee (1992), (*c*) Gatski & Speziale (1993) and (*d*) Shih *et al.* (1992).

shown for the Taulbee (1992), Gatski & Speziale (1993) and Shih *et al.* (1992) models. There are substantial differences between the different models for the β_1-coefficient and a similar behaviour can also be seen for the other coefficients. Figure 5(*a*) is very similar to the results of Pope (1975) although the coefficients in the pressure–strain model were somewhat different.

One should of course bear in mind that the underlying approaches are chosen differently in the different models. This only partly explains the different behaviours though. The Taulbee (1992) model could, however, be directly compared to the implicit ARSM since the basic approach is the Launder *et al.* (1975) model with similar choices of the model coefficients. The classical ARSM assumption is, however, not asymptotically correct for small strain rates and Taulbee thus makes a different approximation in that limit. That difference is clearly seen in the figure. The approximation imposed by Taulbee is motivated by the neglected advection term and gives improved predictions in developing homogeneous shear flows where the advection is important for small times. However, the prediction of fully developed channel flow, where the advection is zero, is also affected by the Taulbee assumption. For that reason this approach is not adopted, even though it improves the predicted shear stresses near the channel centre. A similar effect can be obtained by an approximate inclusion of turbulent diffusion (of a_{ij}) effects, as will be discussed in § 5.

The benefits of a direct, explicit solution of the production to dissipation ratio can be further illustrated by considering rotating plane channel flow. The mean flow is here described by $U(x_2)\delta_{i1}$ and the system rotation is taken as $\omega^s\delta_{i3}$. The mean strain rate tensor is unaffected by system rotation, implying that the effective II_S for the calculation of $\mathscr{P}/\varepsilon$ is the same as for a non-rotating channel flow. The 'effective' second invariant of the mean rotation tensor (see equation (1.14)) becomes

$$II_\Omega^{\mathrm{R}} = \tau^2[-\tfrac{1}{2}\left(U'\right)^2 - 6\left(\tfrac{13}{4}\right)^2(\omega^s)^2 + 2\tfrac{13}{4}\omega^s U']. \tag{2.9}$$

We note that, whereas the first two terms have the same sign on both sides of the channel, the last term has an alternating sign. For moderate rotation rates the model will, thus, predict a decrease of $\mathscr{P}/\varepsilon$ on the side of the channel where II_Ω is increased, and vice versa. This is in agreement with the observed behaviour of a stabilized and a destabilized side in rotating channel flow. Due to the quadratic term (in ω^s) in the expression for II_Ω the model will also predict a global decrease in $\mathscr{P}/\varepsilon$ for very large rates of rotation, as could be expected from comparison with stability theory (see e.g. Matsson & Alfredsson 1990).

2.2. *Solution of the simplified ARSM for three-dimensional mean flow*

For general three-dimensional mean flows the solution for the β-coefficients can be written as

$$\left.\begin{aligned} \beta_1 &= -\frac{N\left(2N^2 - 7II_\Omega\right)}{Q}, \quad \beta_3 = -\frac{12N^{-1}IV}{Q}, \\ \beta_4 &= -\frac{2\left(N^2 - 2II_\Omega\right)}{Q}, \quad \beta_6 = -\frac{6N}{Q}, \quad \beta_9 = \frac{6}{Q}, \end{aligned}\right\} \tag{2.10}$$

where all the other coefficients are identically zero. The denominator

$$Q = \tfrac{5}{6}\left(N^2 - 2II_\Omega\right)\left(2N^2 - II_\Omega\right) \tag{2.11}$$

is also here clearly seen always to remain positive since II_Ω always is negative.

The nonlinear equation for N or the corresponding equation for $\mathscr{P}/\varepsilon$ is for example obtained by introducing the above solution (2.10) for $\boldsymbol{a}$ into the definition of N. The resulting equation is of sixth order and reads

$$N^6 - c_1'N^5 - \left(\tfrac{27}{10}II_S + \tfrac{5}{2}II_\Omega\right)N^4 + \tfrac{5}{2}c_1'II_\Omega N^3 + \left(II_\Omega^2 + \tfrac{189}{20}II_S II_\Omega - \tfrac{81}{5}V\right)N^2 - c_1'II_\Omega^2 N - \tfrac{81}{5}IV^2 = 0. \tag{2.12}$$

This equation reduces to the two-dimensional cubic equation by recalling that in two-dimensional mean flows there are only two independent invariants, whereas $III_S = IV = 0$ and $V = II_S II_\Omega/2$. Equation (2.12) cannot be solved in a closed form but the solution of N for the cubic equation (2.6) applicable in two-dimensional mean flow, N_c, can be used as a first approximation. A further improvement of the approximation of N is also possible by making a perturbation solution of the three-dimensional equation. This is done by perturbing the IV and V invariants around the two-dimensional solution, that is $IV = \sqrt{\phi_1}$ and $V = II_S II_\Omega/2 + \phi_2$, assuming that ϕ_1 and ϕ_2 are independent. Putting this into the three-dimensional equation (2.12) and sorting in powers of ϕ_1 and ϕ_2 we get

$$N = N_c + \frac{162\left(\phi_1 + \phi_2 N_c^2\right)}{D} + O(\phi_1^2, \phi_2^2, \phi_1\phi_2) \tag{2.13}$$

where the denominator, D, is given by

$$D = 20N_c^4\left(N_c - \tfrac{1}{2}c_1'\right) - II_\Omega\left(10N_c^3 + 15c_1'N_c^2\right) + 10c_1'II_\Omega^2 \tag{2.14}$$

where (2.6) has been used to rewrite the expression for D. From (2.14) it is obvious that D will always remain positive, since $N_c \geqslant c_1'$ (see Appendix C).

One could also consider keeping $\mathscr{P}/\varepsilon$ or N implicit during the iteration procedure to a steady-state solution and thus avoid any further approximations. It is, however, not known how this would affect the stability of the numerical method and should be avoided. There could also be problems associated with the existence of multiple roots, especially for three-dimensional cases.

2.2.1. *Example of a three-dimensional mean flow: rotating pipe*

Fully developed turbulent flow in a circular pipe rotating around its length axis is an interesting case, since it represents a three-dimensional flow that can be described with only one spatial coordinate, r in a cylindrical coordinate system ($\hat{\boldsymbol{r}}$, $\hat{\boldsymbol{\theta}}$, $\hat{\boldsymbol{z}}$). If the flow is laminar, the tangential velocity, U_θ, varies linearly with the radius, r, like a solid-body rotation. In turbulent flow, on the other hand, the tangential velocity is nearly parabolic, which cannot be described with an eddy-viscosity turbulence model. The fully three-dimensional form of the proposed EARSM is needed to capture this behaviour. Limited forms with only second-order terms is not sufficient, as will be shown below.

The Navier–Stokes equation in the tangential direction can be written as

$$\nu\left(\frac{\mathrm{d}^2U_\theta}{\mathrm{d}r^2} + \frac{1}{r}\frac{\mathrm{d}U_\theta}{\mathrm{d}r} - \frac{U_\theta}{r^2}\right) = \frac{\mathrm{d}}{\mathrm{d}r}\left(Ka_{r\theta}\right) + 2\frac{Ka_{r\theta}}{r}. \tag{2.15}$$

After two integrations, the tangential velocity can be expressed as

$$U_\theta(r) = U_\theta(R)\frac{r}{R} - \frac{r}{\nu}\int_r^R \frac{Ka_{r\theta}}{u}\mathrm{d}u, \tag{2.16}$$

where R is the radius of the tube. The first term corresponds to the linear U_θ profile while the second term is the correction that may give a parabolic-like profile if the $a_{r\theta}$ anisotropy is positive.

In this particular flow the strain- and rotation-rate tensors are evaluated in an inertial frame and read

$$\boldsymbol{S} = \frac{1}{2}\tau\begin{bmatrix} 0 & \dfrac{\mathrm{d}U_\theta}{\mathrm{d}r} - \dfrac{U_\theta}{r} & \dfrac{\mathrm{d}U_z}{\mathrm{d}r} \\ \dfrac{\mathrm{d}U_\theta}{\mathrm{d}r} - \dfrac{U_\theta}{r} & 0 & 0 \\ \dfrac{\mathrm{d}U_z}{\mathrm{d}r} & 0 & 0 \end{bmatrix} \tag{2.17}$$

and

$$\boldsymbol{\Omega} = \frac{1}{2}\tau\begin{bmatrix} 0 & -\dfrac{\mathrm{d}U_\theta}{\mathrm{d}r} - \dfrac{U_\theta}{r} & -\dfrac{\mathrm{d}U_z}{\mathrm{d}r} \\ \dfrac{\mathrm{d}U_\theta}{\mathrm{d}r} + \dfrac{U_\theta}{r} & 0 & 0 \\ \dfrac{\mathrm{d}U_z}{\mathrm{d}r} & 0 & 0 \end{bmatrix}. \tag{2.18}$$

The terms that contribute to the $a_{r\theta}$ component in the general expression (1.18) are the terms associated with the β_1, β_5, β_6 and β_{10}-coefficients. In the case of a linear U_θ profile, $S_{r\theta}$ is zero and the contribution from the β_1-term vanishes. This is consistent with the behaviour for an eddy-viscosity model.

We see from relation (2.16) that $a_{r\theta}$ should vanish rapidly for increasing Re. To verify that the present EARSM is consistent with such a behaviour we start with the EARSM solution for a flow that may deviate from solid-body rotation. For the present EARSM β_5 and β_{10} are zero, which means that here only the linear term ($\beta_1 \boldsymbol{S}$) and the β_6-term (associated with the $(\boldsymbol{S\Omega}^2 + \boldsymbol{\Omega}^2\boldsymbol{S} - \frac{2}{3}IV\,\boldsymbol{I})$-group) contribute to $a_{r\theta}$:

$$a_{r\theta} = \tfrac{1}{2}\beta_1\tau\left(\frac{\partial U_\theta}{\partial r} - \frac{U_\theta}{r}\right) - \tfrac{1}{4}\beta_6\tau^3\left(\frac{\partial U_\theta}{\partial r} - \frac{U_\theta}{r}\right)\left(\frac{\partial U_\theta}{\partial r} + \frac{U_\theta}{r}\right)^2 - \tfrac{1}{4}\beta_6\tau^3\frac{\partial U_\theta}{\partial r}\left(\frac{\partial U_z}{\partial r}\right)^2. \tag{2.19}$$

For solid body rotation only the third term remains and we see that the $a_{r\theta}$ component will vanish only if the axial mean velocity gradient $\partial U_z/\partial r$ vanishes. This gradient does indeed vanish in the limit of infinite Reynolds number, but only slowly† with increasing Reynolds numbers while the relation (2.16) indicates a more rapid decay rate ($a_{r\theta} \to 1/Re$).

The β_1 and β_6-coefficients in (2.19) are both negative, so the term with the axial mean velocity gradient (the last term) gives a positive contribution to $a_{r\theta}$ which drives the azimuthal velocity $U_\theta(r)$ towards a more parabolic-like profile (where $\partial U_\theta/\partial r > U_\theta/r$). The second term enhances this trend but what is interesting is that the β_1-term (the first term) has the opposite sign and has the possibility of balancing the $a_{r\theta}$ anisotropy component depending on the exact form of the β-coefficients.

Hence, the required consistency of a rapidly vanishing $a_{r\theta}$ is indeed obtained as a solution to the present EARSM, and is in fact associated with a non-zero deviation from solid-body rotation for large but finite Reynolds numbers.

To clearly see this we may need to take a closer look at (2.19) by inserting the present EARSM solutions for β_1, β_6. This gives

$$a_{r\theta} \sim \left(7\frac{U_\theta}{r} - \frac{\partial U_\theta}{\partial r}\right)\left(\frac{\partial U_z}{\partial r}\right)^2 - \left(\frac{\partial U_\theta}{\partial r} - \frac{U_\theta}{r}\right)\left[\frac{81}{4\tau^2}\left(C_1 - 1 + \frac{\mathscr{P}}{\varepsilon}\right)^2 + \left(\frac{\partial U_\theta}{\partial r} + \frac{U_\theta}{r}\right)^2\right] \tag{2.20}$$

and balance is obtained for a parabolic-like profile. Hence, the EARSM solution implies an anisotropy that vanishes much more rapidly than $\partial U_z/\partial r$. As is obvious from (2.20) we also see that in the limit of infinite Re where $\partial U_z/\partial r \to 0$ the vanishing $a_{r\theta}$ is associated with an EARSM solution that gives a solid-body rotation.

The rotation also affects the axial velocity component, which becomes less full, i.e. more parabolic. That effect enters mainly through the rotation dependence in the β_1-coefficient and could thus be captured also by a linear eddy-viscosity model where the C_μ-coefficient is dependent on the rotation rate.

† The 'two-layer hypothesis' $\Rightarrow$ $(U_{CL} - U_z)/u_\tau = f((R-r)/R) \Rightarrow (-(R/U_{CL})(\partial U_z/\partial r))^2 = (-(u_\tau/U_{CL})f')^2 \sim C_f$ where it is also well known that C_f slowly decreases with increasing Reynolds number and that the mean velocity profile in a pipe approaches a top-hat in the infinite Re limit (see e.g. Schlichting 1979, chap. 20).

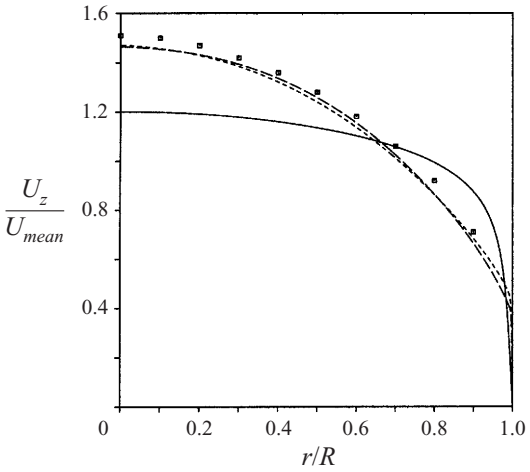

FIGURE 6. Axial velocity in rotating pipe flow for rotation ratio $Z = 1$. Computations with Chien K–ε model (——) and the current EARSM based on Chien K–ε, EARSM_0 (– – –) and EARSM_1 (·····), compared to experiment by Imao *et al.* (1996) (■).

A fully developed turbulent rotating pipe flow has been computed using the proposed model. The Reynolds number is 20 000 based on the mean flow velocity and tube diameter. Three different rotation ratios $Z = 0$, 0.5 and 1 were computed where $Z = U_\theta(R)/U_m$, i.e. the wall angular velocity divided by the axial bulk velocity. The results are compared to the experiment by Imao, Itoh & Harada (1996). The turbulence models used are the Chien (1982) K–ε model and the proposed EARSM including the near-wall formulation in § 3. The EARSM is based on both the K–ε and K–ω models discussed in § 3.4.

The three-dimensional form of the model has been used and the influence of the approximation of N was assessed by computing the case by using both the zeroth- (N_c) and first-order perturbation solution of N. The former is given by (2.7) and labelled 'EARSM_0' in the figures while the latter 'EARSM_1' is given by (2.13).

Figure 6 shows the predicted axial velocity for $Z = 1$ using the Chien K–ε model alone and as the platform for EARSM calculations. The original Chien eddy-viscosity K–ε model is seen to be completely insensitive to rotation, while the EARSM predictions agree well with the experimental results. It is also seen that the different approximations of N only have a minor influence on the predicted velocity profile. In figure 7 predictions for different values of Z are shown for the K–ω model as the platform of the EARSM. The calculated results are seen to capture well the trend with increasing rate of rotation. The EARSM predictions with the K–ε and K–ω platforms are quite similar except in a region close to the wall. The angular velocity (figure 8) is also seen to be reasonably well predicted with the different EARSM formulations, among which the differences are small.

The prediction of the velocity could, however, be improved by the inclusion of the neglected other cubic term associated with β_5 (see (1.18)) and tuning the coefficients for this special case, but it is worth noticing that the results here are obtained without any tuning whatsoever. Moreover, three-dimensional effects driven by turbulence are in most cases quite weak compared to three-dimensional effects driven by mean momentum forces. The rotating pipe is in this case very extreme since the three-dimensional effects are purely turbulence driven.

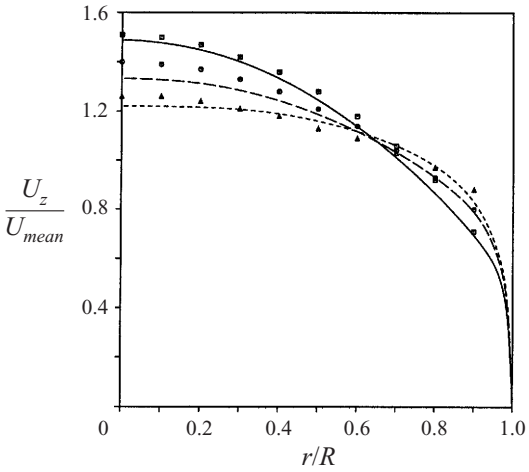

FIGURE 7. Axial velocity in rotating pipe flow for different rotation ratios. Computations with the current EARSM (EARSM_0) based on K–ω (lines) compared to experiment by Imao *et al.* (1996) (symbols) for $Z = 1$ (——) (■), $Z = 0.5$ (– – –) (●) and $Z = 0$ (·····) (▲).

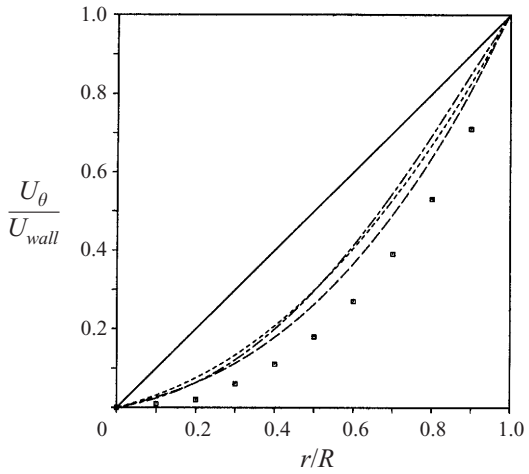

FIGURE 8. Angular velocity in rotating pipe flow for rotation ratio $Z = 1$. Computations with Chien K–ε model (——) and the current EARSM based on Chien K–ε, EARSM_0 (– – –) and EARSM_1 (·····), and the current EARSM (EARSM_0) based on K–ω (–·–·) compared to experiment by Imao *et al.* (1996) (■).

The zeroth- and first-order solutions of N are only different approximations of the exact solution for N or $\mathscr{P}/\varepsilon$. The error can be investigated by computing the $\mathscr{P}/\varepsilon$ ratio using the different approximations of N from a given flow field. Figure 9 shows $\mathscr{P}/\varepsilon$ with N evaluated from the first- (EARSM_0) and second- (EARSM_1) order solutions of N given by (2.7) and (2.13) respectively, compared to the exact solution. The mean flow invariants of these expressions were taken from a fixed mean flow field, which was the solution with EARSM_0 based on K–ε for $Z = 1$. We can see a substantial difference between the zeroth- and first-order solutions and also that the first-order solution is quite close to the exact one. As seen from the previous figures this difference has still a quite small influence on the computed velocity profiles.

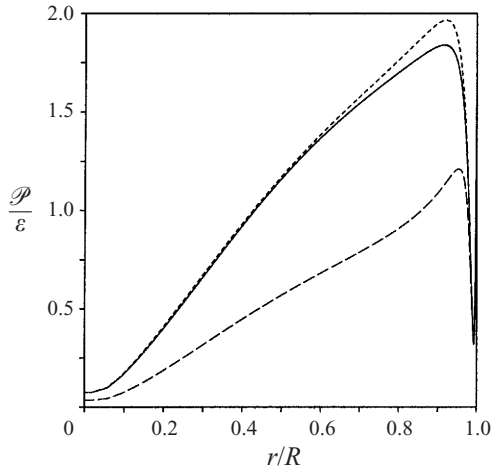

FIGURE 9. Production to dissipation ratio in rotating pipe flow for different approximation levels for N: EARSM_0 (– – –) and EARSM_1 (·····) compared to the exact (——) solution. The mean flow from the EARSM_0 K–ε solution for $Z = 1$ was used.

2.3. *Solution of the general quasi-linear ARSM equation*

So far, the explicit solution of the ARSM resulting from the special case of the Launder *et al.* (1975) model with $c_2 = \frac{5}{9}$ has been analysed. The solution procedure described in this section can, however, be applied to any ARSM that has been derived from a linear or quasi-linear pressure–strain model. Quasi-linear here means that the pressure–strain model must be tensorially linear in $\boldsymbol{a}$ but may contain terms like $\mathrm{tr}\{\boldsymbol{aS}\}\boldsymbol{a}$. The resulting ARSM may be written

$$N\boldsymbol{a} = -A_1\boldsymbol{S} + (\boldsymbol{a\Omega} - \boldsymbol{\Omega a}) - A_2\left(\boldsymbol{aS} + \boldsymbol{Sa} - \tfrac{2}{3}\mathrm{tr}\{\boldsymbol{aS}\}\right) \tag{2.21}$$

where

$$N = A_3 + A_4\frac{\mathscr{P}}{\varepsilon}. \tag{2.22}$$

The solution of (2.21) for three-dimensional mean flow was first derived by Gatski & Speziale (1993) where they considered the production to dissipation ratio as a universal constant which is equivalent to $A_4 = 0$. The fully consistent solution for two-dimensional mean flow was first derived by Girimaji (1996*a*, *b*) where the production to dissipation ratio was obtained as part of the solution.

The solution of (2.21) for three-dimensional mean flow is given in Appendix C. The algebra in that case is considerably more complex than for the simplified ARSM with $c_2 = \frac{5}{9}$. In this section we restrict our attention to two-dimensional mean flow for which the solution for the β-coefficients is

$$\beta_1 = -\frac{A_1 N}{Q}, \quad \beta_2 = 2\frac{A_1 A_2}{Q} \quad \text{and} \quad \beta_4 = -\frac{A_1}{Q}. \tag{2.23}$$

The denominator

$$Q = N^2 - 2II_\Omega - \tfrac{2}{3}A_2^2 II_S \tag{2.24}$$

for this case consists of both positive and negative terms but it can be shown that it is strictly positive due to the fact that N is a function of II_S and II_Ω (see Appendix C).

The Launder *et al.* (1975) model (LRR) is a special case with the A_1 to A_4 coefficients given in table 3. Also, the SSG model by Speziale, Sarkar & Gatski (1991)

LRR	A_1 $\frac{88}{15(7c_2+1)}$	A_2 $\frac{5-9c_2}{7c_2+1}$	A_3 $\frac{11(c_1-1)}{7c_2+1}$	A_4 $\frac{11}{7c_2+1}$
Current model ($c_1 = 1.8, c_2 = \frac{5}{9}$)	1.20	0	1.80	2.25
Original LRR ($c_1 = 1.5, c_2 = 0.4$)	1.54	0.37	1.45	2.89
Linearized SSG	1.22	0.47	0.88	2.37
Gatski & Speziale w/o regularization	1.22	0.47	5.36	0

TABLE 3. The coefficients in the general ARSM for different models.

may be expressed in this form if it is linearized according to Gatski & Speziale (1993). The SSG pressure–strain model reads

$$\frac{\Pi}{\varepsilon} = -\left(\frac{C_1}{2} + \frac{C_1^*}{2}\frac{\mathscr{P}}{\varepsilon}\right)\boldsymbol{a} + \left(C_3 - \frac{C_3^*}{2}\sqrt{II_a}\right)\boldsymbol{S} + \frac{C_4}{2}(\boldsymbol{aS} + \boldsymbol{Sa} - \tfrac{2}{3}\mathrm{tr}\{\boldsymbol{aS}\}\boldsymbol{I}) - \frac{C_5}{2}(\boldsymbol{a\Omega} - \boldsymbol{\Omega a}) + \frac{C_2}{4}(\boldsymbol{a}^2 - \tfrac{1}{3}II_a\boldsymbol{I}), \tag{2.25}$$

where $II_a = \mathrm{tr}\{\boldsymbol{a}^2\}$ and the coefficients are

$$C_1 = 3.4, \quad C_1^* = 1.8, \quad C_2 = 4.2, \quad C_3 = \tfrac{4}{5}, \quad C_3^* = 1.30, \quad C_4 = 1.25, \quad C_5 = 0.40. \tag{2.26}$$

The linearized SSG model used by Gatski & Speziale (1993) is then obtained by neglecting the quadratic anisotropy term and for the II_a invariant they used the equilibrium value predicted by the SSG model for two-dimensional homogeneous turbulence. This results in the following set of coefficients:

$$C_1 = 3.4, \quad C_1^* = 1.8, \quad C_2 = 0, \quad C_3 = 0.36, \quad C_3^* = 0, \quad C_4 = 1.25, \; C_5 = 0.40, \tag{2.27}$$

and A_1 to A_4 are given in table 3. Gatski & Speziale (1993) based their EARSM on this linearized SSG pressure–strain model and implied an additional approximation in order to avoid the nonlinearity in the ARSM equation system. The approximation was to use the asymptotic value for the production to dissipation ratio as a universal constant

$$\frac{\mathscr{P}}{\varepsilon} = \frac{C_{\varepsilon 2} - 1}{C_{\varepsilon 1} - 1} \tag{2.28}$$

which is equivalent to the A_1 to A_4-coefficients given in table 3 for Gatski & Speziale without regularization. The approximation made by Gatski & Speziale (1993) is quite severe, especially since the A_4-coefficient is zero which means that the denominator Q given by (2.24) may become singular. However, in their final expression they have regularized the denominator to avoid the singular behaviour. That form of the model however, could, not exactly be expressed through the A_1 to A_4 coefficients.

The predicted anisotropies in the log-layer and for the asymptotic homogeneous shear flow are listed in tables 4 and 5. The linearized SSG model is able to predict all individual Reynolds stresses fairly well for the two different cases. The Gatski & Speziale (1993) model gives the same result for the asymptotic homogeneous shear but fails in the log-layer since the approximation of the production to dissipation

	a_{12}	a_{11}	a_{22}	a_{33}	σ
DNS	−0.29	0.34	−0.26	−0.08	1.65
Current model ($c_1 = 1.8, c_2 = \frac{5}{9}$)	−0.30	0.25	−0.25	0.00	1.69
Original LRR ($c_1 = 1.5, c_2 = 0.4$)	−0.36	0.26	−0.20	−0.06	1.40
Linearized SSG	−0.32	0.36	−0.26	−0.10	1.59
Gatski & Speziale w/o regularization	−0.29	0.22	−0.16	−0.06	1.75
Gatski & Speziale	−0.28	0.22	−0.16	−0.06	1.76

TABLE 4. The predicted anisotropy in the log-layer using different models assuming balance between turbulence production and dissipation compared to channel DNS (Kim 1989).

	a_{12}	a_{11}	a_{22}	a_{33}	$\mathscr{P}/\varepsilon$
Experiment	−0.30	0.40	−0.28	−0.12	1.8
Current model ($c_1 = 1.8, c_2 = \frac{5}{9}$)	−0.30	0.31	−0.31	0.00	1.8
Original LRR ($c_1 = 1.5, c_2 = 0.4$)	−0.38	0.32	−0.25	−0.07	2.3
Linearized SSG	−0.32	0.41	−0.30	−0.11	1.9
Gatski & Speziale w/o regularization	−0.32	0.41	−0.30	−0.11	1.9
Gatski & Speziale	−0.31	0.41	−0.30	−0.11	1.9

TABLE 5. The predicted anisotropy in homogeneous shear flow using different models with $\sigma = 3.0$ compared to measurements by Tavoularis & Corrsin (1981).

ratio used by them is only consistent for asymptotic shear flows. It should be noted here that the regularization in the Gatski & Speziale model does not influence the solution for these two cases.

The proposed model based on the LRR pressure–strain model is a reasonable choice here due to its simplicity in three-dimensional mean flows, and since the most important anisotropies, namely a_{12} and a_{22}, are fairly well predicted for both the log-layer and for the asymptotic homogeneous shear flow. If better predictions of the a_{11} and a_{33} anisotropies are needed, the linearized SSG may be considered as an alternative but one should realize that this model is considerably more complex for three-dimensional mean flows.

3. Near-wall treatments

In the model presented so far no special attention has been given to the very near-wall region. To obtain the correct behaviour in this region it needs to be modified in a similar way to low Reynolds number two-equation turbulence models. An important difference compared to eddy-viscosity models is that the effective C_μ or β_1 in the proposed model is not a constant and, as has been shown by Wallin & Johansson (1996), will adjust to the near-wall flow in a more natural way than is possible with eddy-viscosity models.

The turbulence timescale $\tau = K/\varepsilon$, which is used to scale the strain- and rotation-rate tensors goes to zero as the wall is approached. A more appropriate expression for the timescale was proposed by Durbin (1993) and reads

$$\tau = \max\left(\frac{K}{\varepsilon}, C_\tau\sqrt{\frac{\nu}{\varepsilon}}\right). \tag{3.1}$$

This is just the usual timescale with a lower bound given by the Kolmogorov scale. Durbin (1993, 1995) uses $C_\tau = 6.0$ which will be kept in this study also.

In the very near-wall region of any shear flow the presence of the solid boundary will enforce a nearly parallel flow except in the immediate vicinity of a separation or stagnation point. A fully developed channel flow is exactly parallel and will be used to formulate and calibrate the very near-wall correction. A specific coordinate system will be used in the derivation of the near-wall correction but the final form is invariant to coordinate system.

In a channel flow, as well as in all parallel flows, we can simply express the anisotropy in terms of the two-dimensional β-terms and the non-dimensional shear, σ, which in parallel flow reads

$$\sigma = \frac{1}{2}\frac{K}{\varepsilon}\frac{\mathrm{d}U}{\mathrm{d}y}. \tag{3.2}$$

The invariants can then simply be expressed as $II_S = 2\sigma^2$ and $II_\Omega = -2\sigma^2$ and the anisotropy becomes

$$a_{12} = \sigma\beta_1, \quad a_{11} = \sigma^2\left(\tfrac{1}{3}\beta_2 - 2\beta_4\right), \quad a_{22} = \sigma^2\left(\tfrac{1}{3}\beta_2 + 2\beta_4\right). \tag{3.3}$$

By letting U in (3.2) represent the velocity along the limiting streamline at the wall the expressions (3.3) can also be said to be approximately valid for three-dimensional near-wall boundary layer flows.

The very near-wall behaviour is studied by using channel DNS data by Kim (1989) at $Re_\delta \approx 7800$ or $Re_\tau \approx 395$. The mean velocity, K and ε profiles obtained from the DNS data have been used to compute the modelled anisotropy, which is compared to the anisotropy determined directly from the DNS data.

The near-wall asymptotic behaviour can be written as

$$\left.\begin{aligned} u^+_{rms} &= a_u y^+ + b_u y^{+2} + \ldots, \\ v^+_{rms} &= a_v y^{+2} + b_v y^{+3} + \ldots, \\ w^+_{rms} &= a_w y^+ + b_w y^{+2} + \ldots, \\ K^+ &= a_K y^{+2} + b_K y^{+3} + \ldots, \\ -\overline{uv}^+ &= a_{uv} y^{+3} + b_{uv} y^{+4} + \ldots\ . \end{aligned}\right\} \tag{3.4}$$

So, Lai & Zhang (1991) summarize these near-wall asymptotic coefficients, $a_u, a_v, \ldots$, for different experimental and numerical near-wall turbulence studies of flat plates, channels and pipes at different Reynolds numbers. These coefficients together with the DNS data by Kim (1989) have been used to calibrate the coefficients in the near-wall corrections.

3.1. *The shear component of the Reynolds stress*

In a channel flow, the mean flow is only directly affected by the Reynolds shear stress, $\overline{uv}$, so let us start by looking at the model of a_{12}.

The modelled a_{12} anisotropy without any near-wall corrections is nearly constant as the wall is approached while DNS data exhibit a behaviour similar to an exponential decay (see figure 10). The obvious choice of 'wall damping function' is of van Driest type

$$f_1 = 1 - \exp\left(-\frac{y^+}{A^+}\right). \tag{3.5}$$

Also shown in figure 10 is the a_{12} behaviour predicted by a standard K–ε model, without any near-wall damping function, which gives strongly negative values near

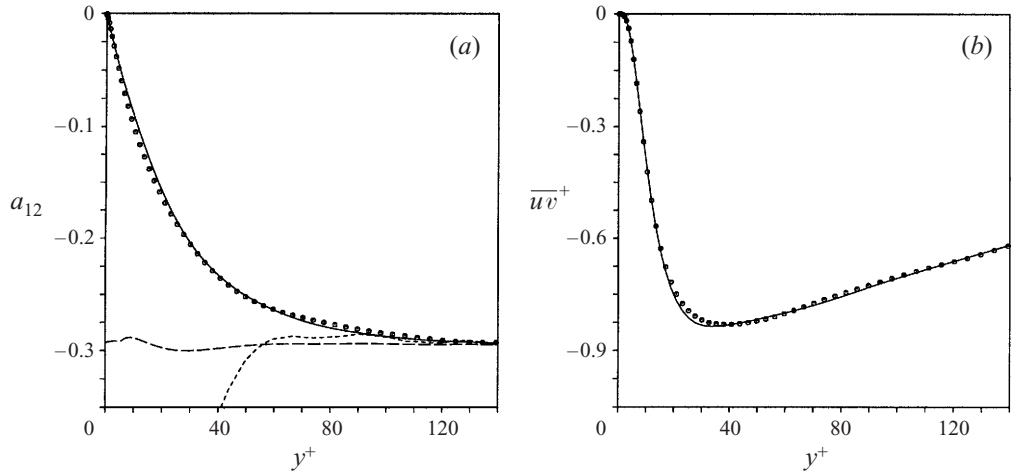

FIGURE 10. a_{12} anisotropy (a) and $\overline{uv}^+$ stress (b) in channel flow. Comparison of the current EARSM with near-wall correction (——) with DNS data (•) (Kim 1989). The computed a_{12} anisotropy using the current EARSM without near-wall correction (– – –) and the eddy-viscosity model (·····) is also shown. The predicted anisotropy was evaluated by use of the DNS data for the $\boldsymbol{S}$ and $\boldsymbol{\Omega}$ fields.

the wall, almost down to -2. Note that this is well outside the range of physically realizable values, that are limited to be between ± 1. The K–ε model cannot be correctly damped towards the wall as easily as the EARSM and the EARSM is therefore much better suited to be integrated down to the wall. This is due to the fact that the β_1-coefficient is not a constant, as in the eddy-viscosity hypothesis, but a function of the mean flow strain rate. In the very near-wall region the strain, normalized by the turbulent timescale, becomes large but the β_1-coefficient goes to zero for large strain rates giving a balanced a_{12} anisotropy (cf. figure 4).

The slope of the a_{12} anisotropy at the wall can be evaluated from the near-wall asymptotic behaviour to be $\partial a_{12}/\partial y^+ = -a_{uv}/a_K$. The constant A^+ varies between 18 and 37 in the data summarized by So *et al.* (1991). By choosing $A^+ = 26$, which also is the standard value in the van Driest function, a good fit to the DNS data is obtained according to figure 10, which shows the corresponding $\overline{uv}$ Reynolds stress. The low Reynolds number coefficient can now be determined as

$$\beta_{1,\text{low-Re}} = f_1 \beta_1, \tag{3.6}$$

where β_1 is the high Reynolds number coefficient obtained from the solution in § 2.

3.2. *The normal components of the Reynolds stress*

The correct near-wall behaviour for the normal Reynolds stresses is then ensured through a correct behaviour of the β_2- and β_4-coefficients. The near-wall asymptotic behaviour of the a_{11} and a_{22} anisotropy is

$$\left.\begin{aligned} a_{11} &= \frac{\overline{u}^2}{K} - \tfrac{2}{3} = \frac{a_u^2}{a_K} - \tfrac{2}{3} + O(y^+), \\ a_{22} &= \frac{\overline{v}^2}{K} - \tfrac{2}{3} = \frac{a_v^2}{a_K} y^{+2} - \tfrac{2}{3} = -\tfrac{2}{3} + O(y^{+2}). \end{aligned}\right\} \tag{3.7}$$

The modelled a_{11} and a_{22} anisotropies, without any wall corrections, are limited near the wall, so a blending of the near-wall asymptote and the outer solution can be

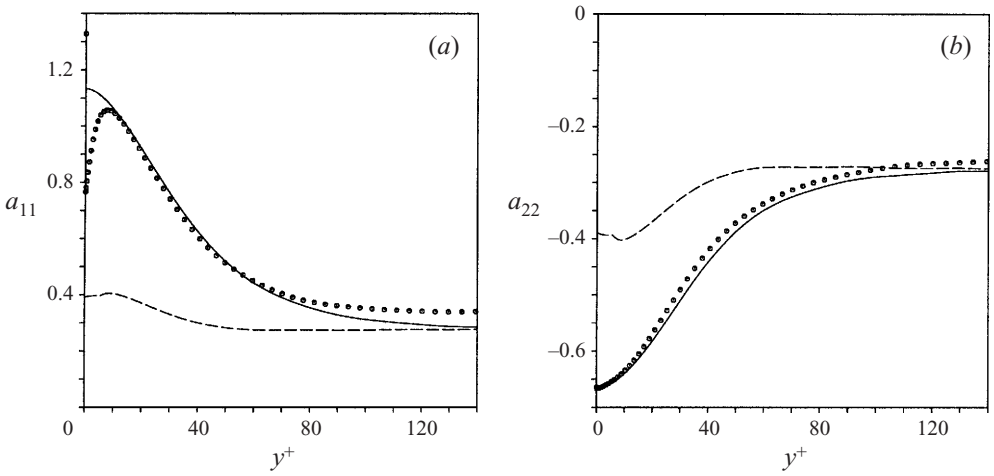

FIGURE 11. a_{11} (*a*) and a_{22} (*b*) anisotropies in channel flow. Comparison of the current EARSM with (——) and without (– – –) near-wall correction with DNS data (•) (Kim 1989). The predicted anisotropy was evaluated by use of the DNS data for the $\boldsymbol{S}$ and $\boldsymbol{\Omega}$ fields.

done. For simplicity, the same blending function, f_2, is used for the both anisotropies, which become

$$\left.\begin{aligned} a_{11,\text{low-Re}} &= f_2 a_{11} + (1-f_2)\left(B_2 - \tfrac{2}{3}\right), \\ a_{22,\text{low-Re}} &= f_2 a_{22} + (1-f_2)\left(-\tfrac{2}{3}\right), \end{aligned}\right\} \tag{3.8}$$

where $B_2 = a_u^2/a_K$. Equation (3.7) states that a_{22} has zero slope at the wall so the function f_2 must also have zero slope. A simple choice that satisfies this criterion is $f_2 = f_1^2$. The low Reynolds number coefficients then become

$$\beta_{2,\text{low-Re}} = \frac{3B_2 - 4}{2\sigma^2}\left(1 - f_1^2\right), \quad \beta_{4,\text{low-Re}} = f_1^2\beta_4 - \frac{B_2}{4\sigma^2}\left(1 - f_1^2\right), \tag{3.9}$$

where β_4 is the high Reynolds number coefficient obtained from the solution in § 2.

The constant B_2 can be evaluated using the data summarized by So *et al.* (1991) and varies between 1.56 and 1.84. By choosing $B_2 = 1.8$ a good fit to the DNS data is obtained (see figures 11 and 12).

3.3. *Extension to general flows*

The near-wall correction described so far was obtained for a special case, namely parallel two-dimensional flows, and cannot directly be generalized to three-dimensional mean flows. Some singularities in flows near separation must be considered and the formulation needs to be written in a coordinate-system-invariant form. These additional extensions must be formulated such that the original form above is retained for parallel two-dimensional flows.

So far, the near-wall correction is described in terms of σ, which is defined in (3.2) for a specific coordinate system. By using $II_S = 2\sigma^2$, a coordinate-system-invariant form of the near-wall correction can be obtained. In separated flow the shear rate σ may become small, leading to a singular behaviour of the near-wall corrections to the β_2- and β_4-coefficients. To avoid this problem, the shear rate in the denominator of the near-wall correction is limited to the equilibrium shear rate where the turbulence production balances the dissipation rate. The near-wall shear rate is always larger

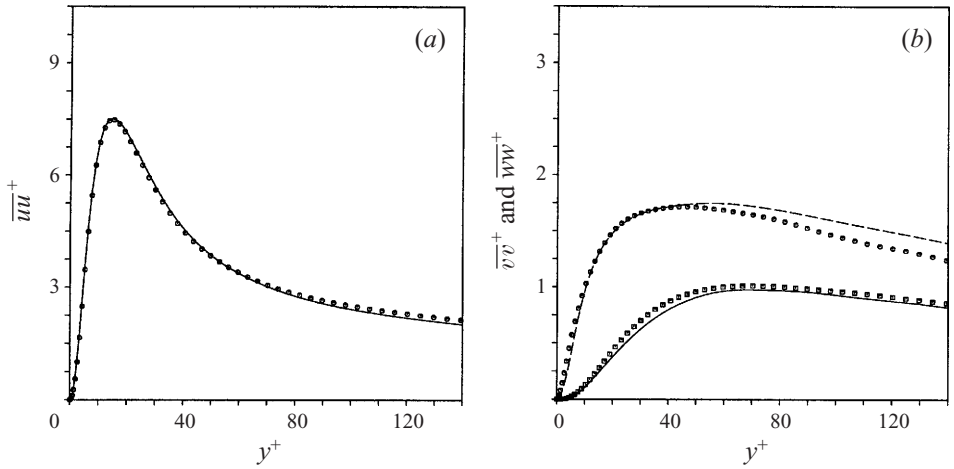

FIGURE 12. Reynolds stresses in channel flow. Comparison of the current EARSM, $\overline{uu}^+$ (——) (*a*) and $\overline{vv}^+$ (——), $\overline{ww}^+$ (– – –) (*b*), with DNS data, (■) and (•), (Kim 1989). The predicted anisotropy was evaluated by use of the DNS data for the $\boldsymbol{S}$ and $\boldsymbol{\Omega}$ fields.

than the equilibrium one in zero pressure gradient flows and the limiter will only be active in flows near separation. The anisotropy model including the near-wall formulation then reads

$$\boldsymbol{a} = f_1\beta_1\boldsymbol{S} + \left(1 - f_1^2\right)\frac{3B_2 - 4}{\max\left(II_S, II_S^{\mathrm{eq}}\right)}\left(\boldsymbol{S}^2 - \tfrac{1}{3}II_S\,\boldsymbol{I}\right) + \left(f_1^2\beta_4 - \left(1 - f_1^2\right)\frac{B_2}{2\max\left(II_S, II_S^{\mathrm{eq}}\right)}\right)\left(\boldsymbol{S\Omega} - \boldsymbol{\Omega S}\right), \quad (3.10)$$

where II_S^{eq} is the equilibrium value obtained by setting $\mathscr{P} = \varepsilon$ in the two-dimensional solution and reads $II_S^{\mathrm{eq}} = 405c_1^2/(216c_1 - 160) \approx 5.74$ for $c_1 = 1.8$. The β-coefficients are given by equation (2.5) and f_1 is given by equation (3.5). Please observe that even though the high Reynolds number β_2-coefficient is zero the tensor group associated with the β_2-coefficient does not vanish.

The straightforward extension to three-dimensional flow reads

$$\begin{aligned}\boldsymbol{a} = {} & f_1\beta_1\boldsymbol{S} + \left(1 - f_1^2\right)\frac{3B_2 - 4}{\max\left(II_S, II_S^{\mathrm{eq}}\right)}\left(\boldsymbol{S}^2 - \tfrac{1}{3}II_S\,\boldsymbol{I}\right) \\ & + f_1^2\beta_3\left(\boldsymbol{\Omega}^2 - \tfrac{1}{3}II_\Omega\,\boldsymbol{I}\right) + \left(f_1^2\beta_4 - \left(1 - f_1^2\right)\frac{B_2}{2\max\left(II_S, II_S^{\mathrm{eq}}\right)}\right)\left(\boldsymbol{S\Omega} - \boldsymbol{\Omega S}\right) \\ & + f_1\beta_6\left(\boldsymbol{S\Omega}^2 + \boldsymbol{\Omega}^2\boldsymbol{S} - \tfrac{2}{3}IV\,\boldsymbol{I}\right) + f_1^2\beta_9\left(\boldsymbol{\Omega S\Omega}^2 - \boldsymbol{\Omega}^2\boldsymbol{S\Omega}\right). \end{aligned} \quad (3.11)$$

This form reduces to (3.10) for two-dimensional mean flows.

The near-wall correction is strictly valid only for parallel two-dimensional mean flow but the very near-wall flow is, however, near parallel and two-dimensional also for quite complex three-dimensional flow fields so the equation (3.11) can be used as a first approximation. The correction can be extended to also be valid for flows near stagnation points like separation and reattachment points, for flows over curved surfaces and also for three-dimensional mean flows. This extension of the near-wall

correction is, however, outside the scope of this paper but will be addressed in future studies.

3.4. *Length-scale determining equation*

So far, we have proposed a new explicit constitutive relation between the mean flow strain rate and the Reynolds stresses including near-wall treatments. The choice of velocity- and length-scale determining equations has not yet been discussed. The turbulent kinetic energy, K, is a natural choice for determining the turbulent velocity-scale since this equation needs no further modelling. The dissipation of the turbulent kinetic energy, ε, is the most commonly used quantity for determining the turbulent length-scale but other alternatives are also possible like τ and ω.

Common to all length-scale determining equations is that they need a lot of *ad hoc* modelling, substantially more than the K-equation. The different terms are quite empirical and are tuned for specific flow cases. There are many different K–ε models with the major differences in the near-wall modelling in the ε-equation and in the eddy-viscosity relation. Most of the ε-models are also tuned and calibrated together with the eddy-viscosity assumption, which gives a poor description of the near-wall anisotropy. One should thus not be surprised if the proposed EARSM together with an existing length-scale model does not give any improvements and perhaps also worse capabilities in predicting basic wall-bounded flows.

The correct methodology to obtain a length-scale determining equation is to develop it from scratch together with the proposed EARSM, so that one avoids the risk of inheriting terms that are needed to balance the errors introduced by the eddy-viscosity assumption. This is, however, outside the scope of this paper but will be addressed in future studies. For an illustration of the capability of the proposed model and to obtain an indication of how different length-scale determining equations act, we have tested the proposed model together with the well known Chien (1982) K–ε model and the Wilcox (1994) K–ω model for the fully developed channel case simulated by Kim (1989).

In these computations we did not use the Daly & Harlow model, equation (1.17), of the diffusion terms in the K and ε (or ω) equations. The approach was to use the standard eddy-viscosity modelling of the diffusion term but with an effective C_μ evaluated from the EARSM such as $C_\mu^{\text{eff}} = -f_1\beta_1/2$. The differences between the Daly & Harlow and the eddy-viscosity approaches were found to be small for the K–ε model as long as the effective C_μ is used rather than a constant. In case of the K–ω model, the turbulent diffusion is complete different compared to that of the K–ε model and thus the Daly & Harlow approach needs to be recalibrated. The eddy-viscosity approach could, however, directly be used also here as long as the effective C_μ (or β^*) is used. In three-dimensional mean flows the effective C_μ is $C_\mu^{\text{eff}} = -f_1(\beta_1 + II_\Omega\beta_6)/2$

Figures 13 to 18 show the result of the computations with the two different two-equation models based on the proposed EARSM as well as with the original eddy-viscosity assumption. The EARSM has been used both with the original and modified ('mod') length-scale equations.

If we first look at the velocity profiles in figure 13 one finds that the additive constant B in the log-law is much too high when the EARSM is used. This clearly illustrates the need for recalibration discussed above. The figure also shows the results when the length-scale equation is tuned or modified to better match the log-law. In

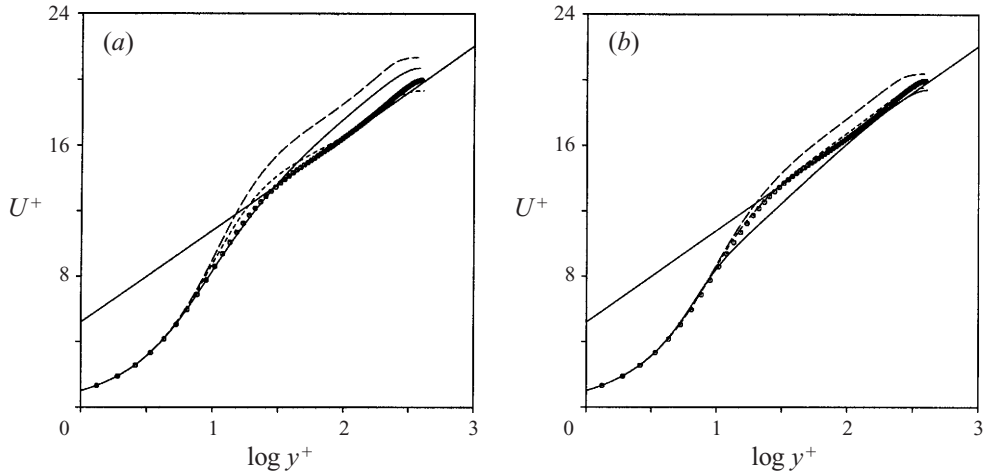

FIGURE 13. The streamwise velocity in channel flow. Computations based on Chien K–ε (*a*) and K–ω (*b*) using eddy viscosity (——) and the current EARSM with the original (– – –) and modified (·····) ε and ω equations compared with DNS data (•) (Kim 1989) and the log-law (——).

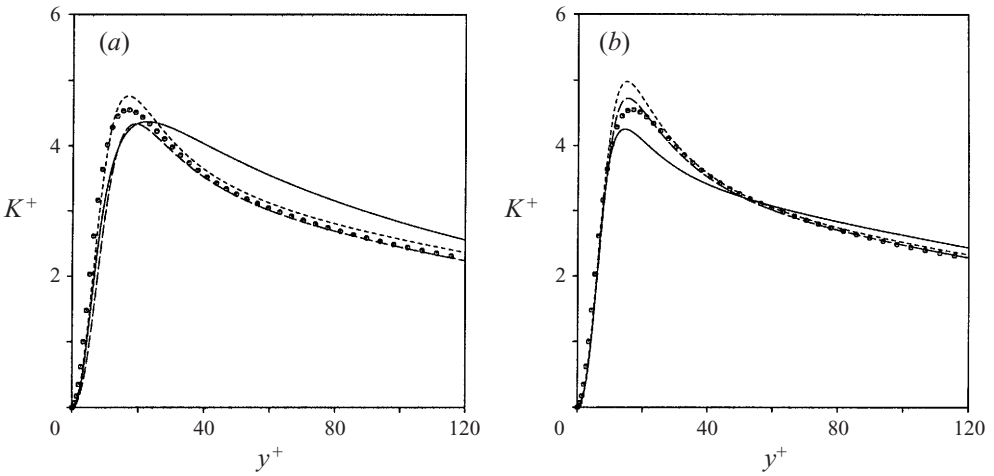

FIGURE 14. The turbulent kinetic energy in channel flow. Computations based on Chien K–ε (*a*) and K–ω (*b*) using eddy viscosity (——) and the current EARSM with the original (– – –) and modified (·····) ε and ω equations compared with DNS data (•) (Kim 1989).

the K–ε model the definition of ε in Chien's model has been changed to

$$\varepsilon = \tilde{\varepsilon} + \frac{2\nu K}{y^2} \exp\left(-C_k y^+\right), \tag{3.12}$$

where the constant $C_k = 0.04$. This means that the original 'wall dissipation' is multiplied by an exponential function to give a more rapid decay of the modification near the wall. In the Wilcox K–ω model, the constant R_β was increased from 8 to 10 to obtain the desired behaviour. For a more thorough comparison between K–ε and K–ω models the reader may wish to consult Menter (1994).

It is also interesting to note the clear improvement in the K-profiles with the proposed EARSM both for the K–ε and K–ω models in figure 14. The near-

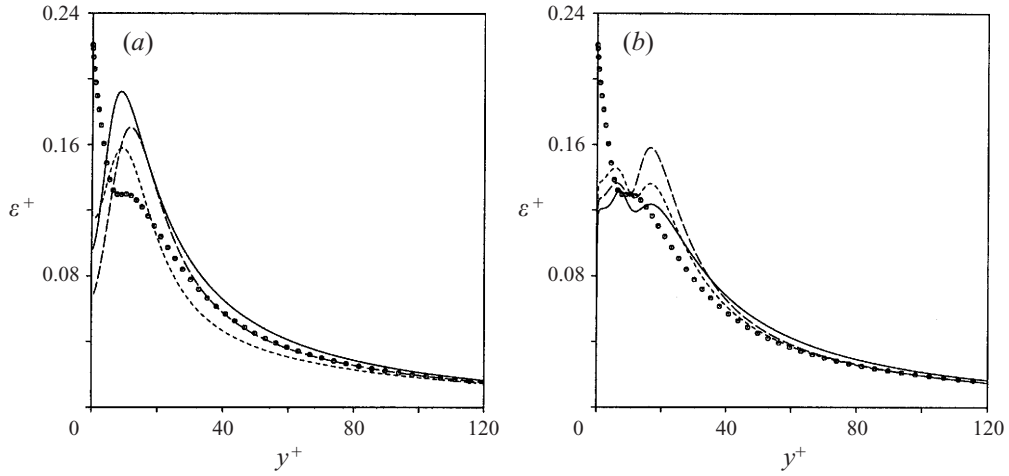

FIGURE 15. The dissipation of turbulent kinetic energy in channel flow. Legend as in figure 14.

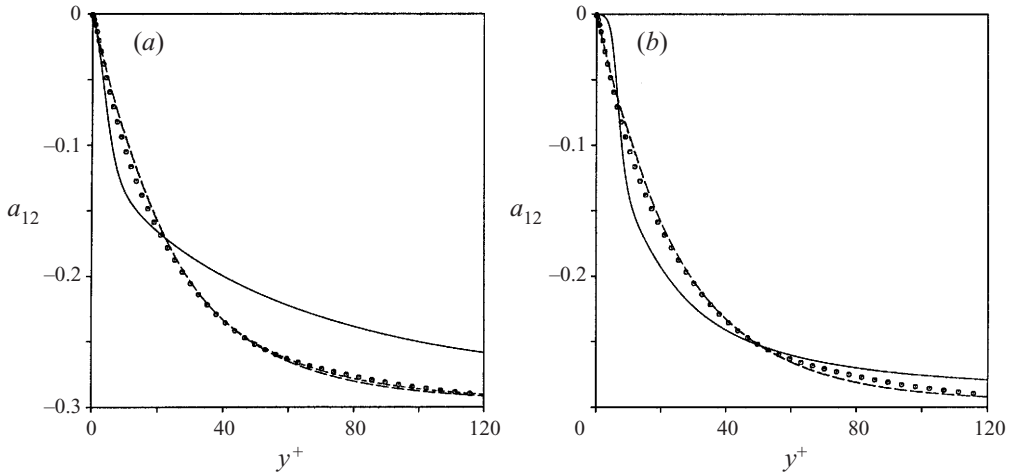

FIGURE 16. The a_{12} anisotropy in channel flow. Legend as in figure 14.

wall dissipation ratio shown in figure 15 illustrates the need for a better near-wall modelling of the length-scale equation. In figures 16 to 18 we can see the good near-wall behaviour of the proposed EARSM which seems to be quite insensitive to the choice of basic two-equation model. In figure 16 we can also clearly see how poorly the a_{12} anisotropy is predicted with the eddy-viscosity models.

The rotating pipe flow discussed in § 2.2.1 was computed with these two models (K–ε and K–ω) as platforms for EARSM. Figures 6 and 7 show that differences are seen in a region close to the wall, where the K–ε based model shows a higher wall shear stress than the K–ω based model. The latter correctly captures the trend of a decreasing skin friction with increasing rate of rotation, whereas the K–ε based EARSM gives the opposite trend.

3.5. *Alternative near-wall scaling*

The damping function, f_1 given by equation (3.5), is formulated in terms of y^+. The scaling with the local wall skin friction is not valid in flows near separation and

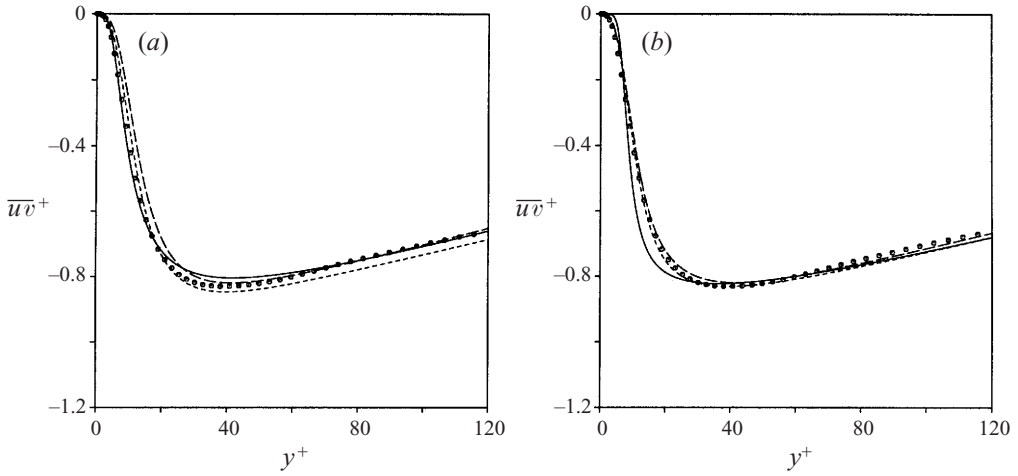

FIGURE 17. The $\overline{uv}^+$ Reynolds stress in channel flow. Legend as in figure 14.

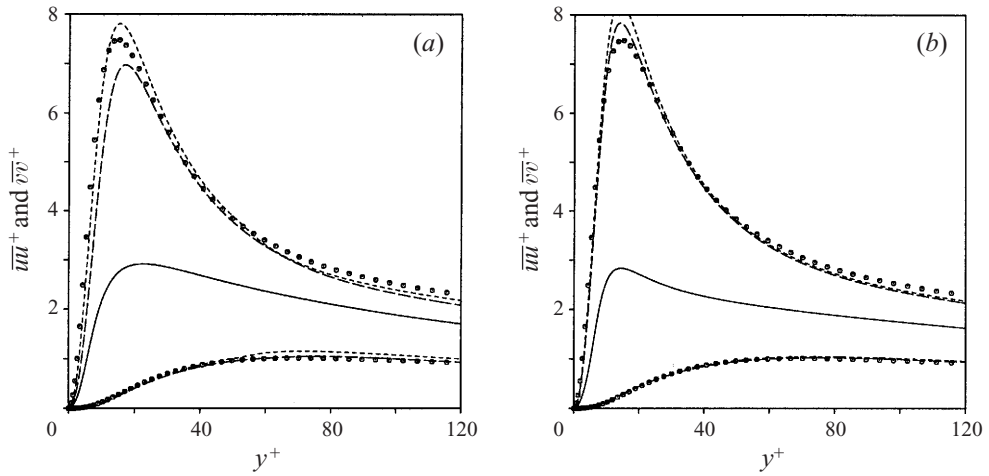

FIGURE 18. The normal Reynolds stresses in channel flow. Legend as in figure 14.

reattachment. Other possibilities than y^+ are $Re_y \equiv \sqrt{K}y/\nu$ or the turbulent Reynolds number $Re_t \equiv K^2/\nu\varepsilon$ (see e.g. Wilcox 1993).

The approach is here to formulate an alternative scaling y^* in terms of Re_y or Re_t so that $y^* \approx y^+$ for $y^+ \leqslant 100$ in channel flows. Re_y and Re_t were computed from DNS data at different Reynolds numbers ranging from $Re_\tau = 150$ to 650 in channel flows (Moser, Kim & Mansour 1998) and zero pressure gradient boundary layers (Spalart 1988). It was found that Re_y was increasing from the wall more linearly with less scattering compared to Re_t. Moreover, it should not pose any major problems to compute the wall distance y needed for Re_y if that is defined as the distance to the closest wall point. The following form for y^* is thus proposed:

$$y^* = C_{y1}\sqrt{Re_y} + C_{y2}Re_y^2. \tag{3.13}$$

The $\sqrt{Re_y}$-term is motivated by the fact that the near-wall asymptotic behaviour for Re_y is $\sim y^2$. The Re_y^2-term is artificially introduced to obtain a near linear relation

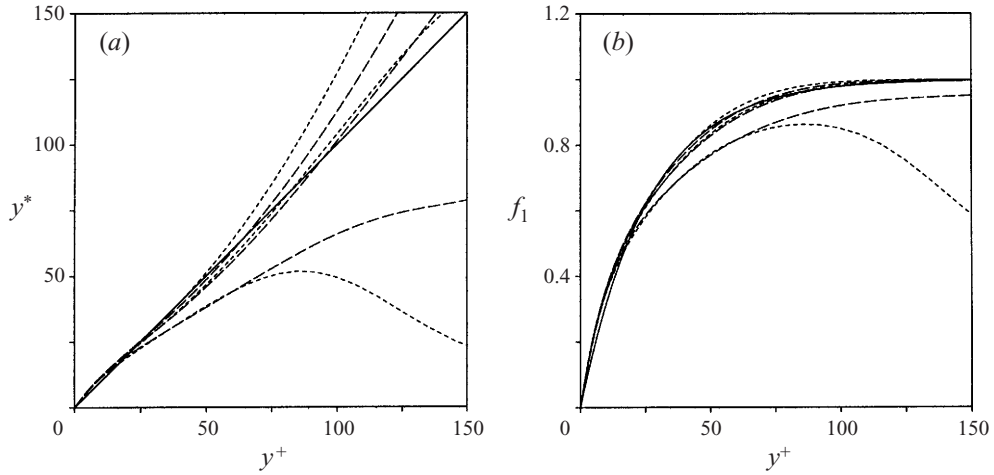

FIGURE 19. (*a*) The near-wall scaling y^* compared to y^+. (*b*) The damping function f_1 using y^* or y^+. The original form using y^+ (——) is compared to channel DNS data (Moser *et al.* 1998) at different Reynolds numbers $Re_\tau = 180$, 395 and 590 (– – –) and zero pressure gradient boundary layer DNS data (Spalart 1988) at $Re_\tau = 150$, 325 and 650 (·····). y^* increases with increasing Reynolds number.

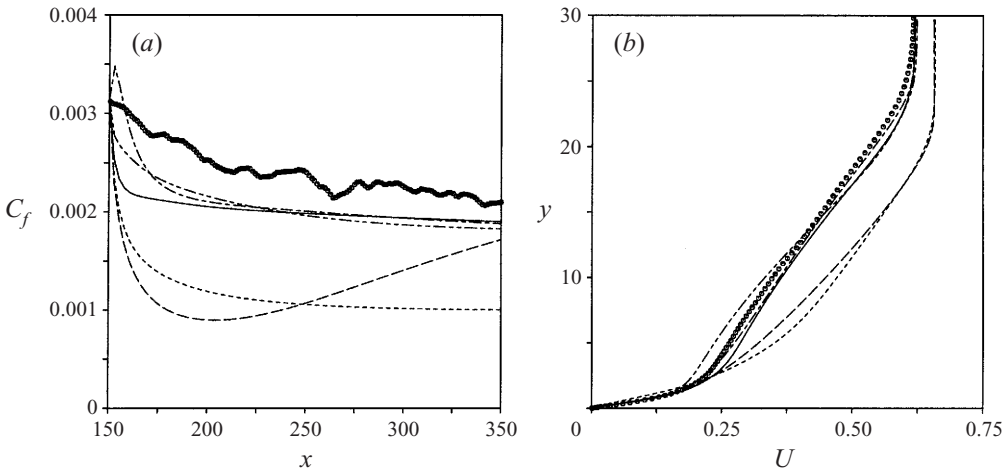

FIGURE 20. (*a*) The wall skin friction and (*b*) the velocity profile for an adverse pressure gradient boundary layer ($U_\infty \sim x^{-0.25}$). Computations with standard Wilcox (1988) K–ω (– · –), Chien K–ε (– – –), EARSM based on K–ω and y^+ (·····) or y^* (——) and the Hanjalić (1995) RST model (– · · –). Comparisons with DNS data (•), M. Skote (private communication).

in the buffer region also. With $C_{y1} = 2.4$ and $C_{y2} = 0.003$ good agreement with y^+ for channel and zero pressure gradient boundary layer flows at different Reynolds numbers is obtained, see figure 19.

In the damping function f_1, y^+ is then replaced by y^*

$$f_1 = 1 - \exp\left(-\frac{y^*}{A^+}\right). \tag{3.14}$$

In figure 19 the damping function f_1 based on y^* is compared to f_1 based on y^+. The correspondence is good except for the lowest Reynolds numbers.

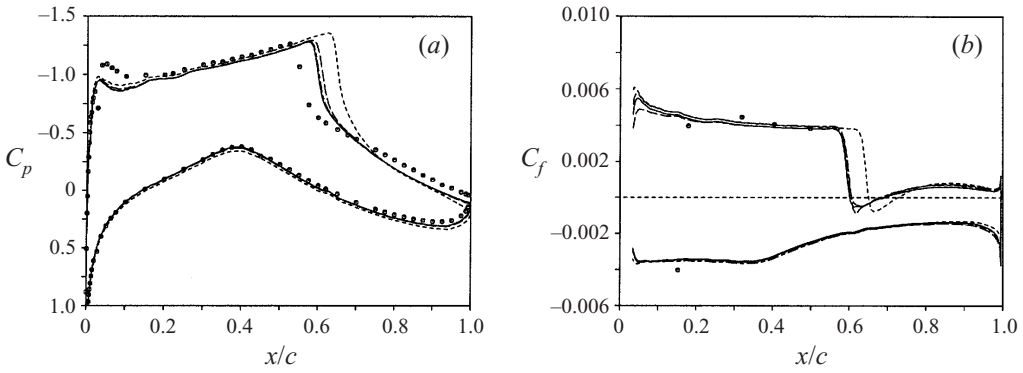

FIGURE 21. (*a*) Wall pressure and (*b*) skin friction coefficients for the RAE2822 wing profile ($M = 0.754$, $\alpha = 2.57°$ and $Re = 6.2 \times 10^6$). Predictions using Wilcox (1994) K–ω (·····) and the current EARSM based on K–ω with damping function based on y^+ (– – –), y^* (——) or without any damping functions (–·–·), compared to experimental data (•) (Cook *et al.* 1979). The geometry is the measured one including a camber correction.

In some situations the y^+ scaling may worsen the computational results. In a forthcoming study by M. Skote adverse pressure gradient boundary layers are studied by DNS. For the highest pressure gradient studied, with the pressure gradient similarity parameter $m = -0.25$ ($U_\infty \sim x^m$), the difference between the y^+ and y^* approaches are significant here, see figure 20. For this case it is obvious that the y^+ scaling degenerates the model performance and should be avoided.

In other cases, where the Reynolds number is higher, the near-wall scaling is not as critical. Figure 21 shows the computational results for the two-dimensional RAE2822 aerofoil profile using the proposed EARSM compared to the Wilcox (1994) K–ω model. The flow in this case is compressible and the formulation is modified in a manner described in §4. The EARSM approach clearly improves the position of the shock and the results are very much in line with differential Reynolds stress computations by Hellström, Davidson & Rizzi (1994) for exactly the same conditions and geometry.

The damping function in the EARSM is formulated in terms of y^+ as well as y^* and the figure shows no major differences between these approaches except in the separated region where the y^+ formulation gives a somewhat larger negative skin friction. In the figure a computation using the proposed EARSM without any damping functions whatsoever is also shown. For that choice, the standard Wilcox (1988) K–ω, also without damping functions, must be used as the platform. This combination gives, however, incorrect near-wall behaviour for the turbulence quantities but the mean velocity profiles are well reproduced. That is also seen in the figure where no major differences between the EARSM with or without damping functions are present.

The convergence history is shown in figure 22 where we can see that there are no major differences in convergence rate. Actually, the proposed EARSM converges to a somewhat lower residual than the corresponding eddy-viscosity model for this case. The numerical parameters are the same for these two cases and the computational time for the 5000 iteration steps is 6% higher for the EARSM computation. This case was found to be not completely numerically stationary which results in the residual 'hanging' as for the K–ω model. The fluctuations are, however, very small and could not be seen in the solution. In other cases without separation the convergence curves are even closer to each other, and the convergence rates are in general faster than

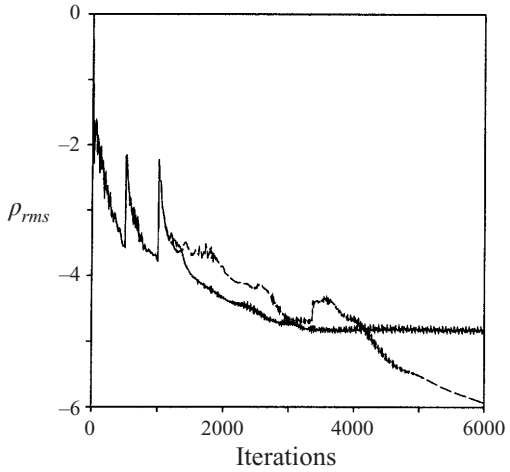

FIGURE 22. Convergence history for the RAE2822 wing profile. Wilcox K–ω (——) compared with the current EARSM based on K–ω (– – –). The computational time is increased by 6% by using EARSM. Three levels of full multigrid is used.

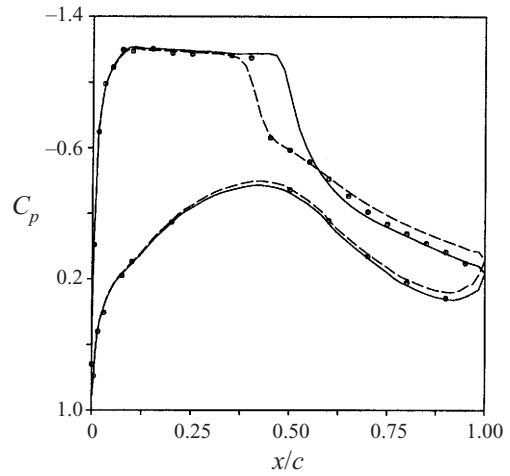

FIGURE 23. Wall pressure coefficient C_p for the LANN-wing ($M = 0.82$, $\alpha = 2.59^\circ$ and $Re = 5.4 \times 10^6$) at the spanwise position of 0.474. Predictions using Wilcox (1988) K–ω (——) and the current EARSM (– – –) based on K–ω without wall damping functions. Comparison with experimental data (•) (Horsten *et al.* 1983).

for the case shown in figure 22. The computational results were obtained using the EURANUS code by Rizzi *et al.* (1993) which is an explicit time-stepping multigrid and multiblock Navier–Stokes solver. The grid convergence was assessed by repeating the computation on a coarser grid.

A further example is a three-dimensional transonic supercritical wing (figure 23). This case is computed using the standard Wilcox (1988) K–ω model and the EARSM based on that. Since that K–ω model has no damping functions the EARSM without damping functions must also be used for consistency. Again, the predicted shock position is improved compared to the eddy-viscosity model. This case illustrates the benefit of the proposed model which is also viable in expensive three-dimensional

cases, here with almost one million grid points. Most importantly, there is no substantial increase in the computational cost compared to the, in many cases, robust standard K–ω model.

4. Compressibility

Many turbulent flow applications are within the Mach number regime where compressible effects must be considered. Also, in low speed flow compressible effects may be important due to local heating or cooling of the flow. Compressible turbulent flow may be classified according to Friedrich & Bertolotti (1997) into flows with vanishing compressibility effects due to turbulent fluctuations and flows where such effects play a significant role. Friedrich & Bertolotti (1997) also states that compressibility effects due to turbulent fluctuations might be important in hypersonic, high Mach number, wall-bounded flows and in mixing layers at high convective Mach numbers. The understanding of such flows is poor and models capable of distinguishing the principal differences between wall-bounded and free shear flows are not well developed. The compressibility effects, due to turbulent fluctuations, increase the anisotropy of the Reynolds stress tensor (see Friedrich & Bertolotti 1997) and depend themselves on the anisotropy, which means that algebraic Reynolds stress models are better suited than eddy-viscosity models to act as a basis for improving the prediction of compressibility effects.

In wall-bounded flows with Mach numbers below 5 compressibility effects due to turbulent fluctuations may be neglected and the effect of compressibility enters into the problem essentially only through the mean flow compressibility. In this study we will restrict attention to this class of flows and a straightforward compressibility extension of the incompressible model will be made.

First, the stress anisotropy and the turbulent kinetic energy must be redefined as $a_{ij} \equiv \overline{\rho u_i u_j}/\rho K - 2\delta_{ij}/3$ and $K \equiv \overline{\rho u_i u_i}/2\rho$ where ρ is the local mean density of the fluid. The trace of the strain is not zero for compressible flow. We may instead use a somewhat redefined normalized strain rate tensor

$$S_{ij} \equiv \frac{\tau}{2}\left(U_{i,j} + U_{j,i}\right) - \frac{\mathscr{D}}{3}\delta_{ij}, \tag{4.1}$$

where the normalized dilatation of the mean flow is defined as $\mathscr{D} \equiv \tau U_{k,k}$.

The redefinition of $\boldsymbol{S}$ to have zero trace allows us to make use of the incompressible solution process. The redefinition also implies, however, that the S_{33}-component is non-zero for two-dimensional mean flow in the (x, y)-plane and that the simplifications for two-dimensional mean flow are not strictly valid for compressible flow. This will be addressed as a special case later in this section.

The general linear model of the LRR rapid pressure–strain rate model for incompressible flow does not have zero trace in compressible flow, so the model needs to be generalized according to Vandromme (1992) and reads

$$\Pi_{ij}^{(r)} = -\frac{c_2+8}{11}(\mathscr{P}_{ij} - \tfrac{2}{3}\mathscr{P}\delta_{ij}) - \frac{30c_2-2}{55}\rho K \times(U_{i,j} + U_{j,i} - \tfrac{2}{3}U_{l,l}\delta_{ij}) - \frac{8c_2-2}{11}(D_{ij} - \tfrac{2}{3}\mathscr{P}\delta_{ij}), \tag{4.2}$$

where $\mathscr{P}_{ij} = -\overline{\rho u_i u_k}U_{j,k} - \overline{\rho u_j u_k}U_{i,k}$ and $D_{ij} = -\overline{\rho u_i u_k}U_{k,j} - \overline{\rho u_j u_k}U_{k,i}$. The incompressible models for the slow pressure–strain and the dissipation tensor can also be used

here. The general ARSM for compressible flow can now be written as

$$\left(c_1 - 1 - \frac{6c_2+4}{11}\mathscr{D} - \mathrm{tr}\{\boldsymbol{aS}\}\right)\boldsymbol{a} = -\tfrac{8}{15}\boldsymbol{S} + \frac{7c_2+1}{11}(\boldsymbol{a\Omega}-\boldsymbol{\Omega a}) - \frac{5-9c_2}{11}\left(\boldsymbol{aS}+\boldsymbol{Sa}-\tfrac{2}{3}\mathrm{tr}\{\boldsymbol{aS}\}\boldsymbol{I}\right) \quad (4.3)$$

which is identical to the incompressible form, equation (1.13), except for the dilatation term on the left-hand side and the different definitions given above. The same conclusion is valid for the simplified equation obtained by setting $c_2 = \frac{5}{9}$, which reads

$$\left(c_1 - 1 - \tfrac{2}{3}\mathscr{D} - \mathrm{tr}\{\boldsymbol{aS}\}\right)\boldsymbol{a} = -\tfrac{8}{15}\boldsymbol{S} + \tfrac{4}{9}(\boldsymbol{a\Omega}-\boldsymbol{\Omega a}). \quad (4.4)$$

The solution of the simplified compressible ARSM equation is the same as the incompressible solution except for the definition of the c_1'-coefficient, which for the compressible case is

$$c_1' = \tfrac{9}{4}\left(c_1 - 1 - \tfrac{2}{3}\mathscr{D}\right) \quad (4.5)$$

bearing in mind that S_{ij} here is defined by (4.1).

4.1. *Compressible two-dimensional mean flow*

An approximation of the compressible ARSM equation can be derived by an expansion around a solution obtained by use of the two-dimensional simplification valid in incompressible flow. Let us first define a compressible two-dimensional strain rate as $S_{ij}^{2D} \equiv (\tau/2)\left(U_{i,j}+U_{j,i}\right) - \mathscr{D}\delta_{ij}^{2D}/2$ where $\delta_{ij}^{2D} \equiv \delta_{ij}$ except that $\delta_{33}^{2D} = 0$. The compressible ARSM, equation (4.4), can now be written as

$$\left(c_1 - 1 - \tfrac{2}{3}\mathscr{D} - \mathrm{tr}\{\boldsymbol{a}^{2D}\boldsymbol{S}^{2D}\}\right)\boldsymbol{a}^{2D} = -\tfrac{8}{15}\boldsymbol{S}^{2D} + \tfrac{4}{9}\left(\boldsymbol{a}^{2D}\boldsymbol{\Omega} - \boldsymbol{\Omega a}^{2D}\right) \quad (4.6)$$

with the solution $\boldsymbol{a}^{2D}$, which is derived using the two-dimensional solution process for incompressible flow. The true anisotropy, $\boldsymbol{a}$, is then related to the solution $\boldsymbol{a}^{2D}$, as described below.

The difference between $\boldsymbol{S}$ and $\boldsymbol{S}^{2D}$ is of $O(\mathscr{D})$ which can be assumed small except in a shock wave. For the same reason the difference between $\boldsymbol{a}$ and $\boldsymbol{a}^{2D}$ can also be assumed to be of $O(\mathscr{D})$ and with the simplest tensorial form that relates the two-dimensional and three-dimensional anisotropies, leading to the following assumption. Let

$$\boldsymbol{a} = \boldsymbol{a}^{2D} + \beta_a\mathscr{D}\left(\boldsymbol{I}^{2D} - \tfrac{2}{3}\boldsymbol{I}\right) + O(\mathscr{D}^2), \quad (4.7)$$

and subtract equation (4.6) from equation (4.4). Sorting terms in powers of $\mathscr{D}$ gives us the first-order solution in $\mathscr{D}$

$$\beta_a = -\frac{4}{15\left(c_1 - 1 - \mathrm{tr}\{\boldsymbol{a}^{2D}\boldsymbol{S}^{2D}\}\right)}. \quad (4.8)$$

In obtaining this solution the following relations have been used:

$$\left.\begin{aligned} \boldsymbol{S}^{2D} &= \boldsymbol{S} - \tfrac{1}{2}\mathscr{D}\left(\boldsymbol{I}^{2D} - \tfrac{2}{3}\boldsymbol{I}\right) \\ \mathrm{tr}\{\boldsymbol{a}^{2D}\boldsymbol{S}^{2D}\} &= \mathrm{tr}\{\boldsymbol{aS}\} + O(\mathscr{D}^2) \\ \boldsymbol{a}^{2D}\boldsymbol{\Omega} - \boldsymbol{\Omega a}^{2D} &= \boldsymbol{a\Omega} - \boldsymbol{\Omega a} + O(\mathscr{D}^2). \end{aligned}\right\} \quad (4.9)$$

The zeroth-order solution, $\boldsymbol{a}^{2D}$, is obtained as described for the incompressible case, with the only difference being that c_1' is now given by (4.5). The full solution is then

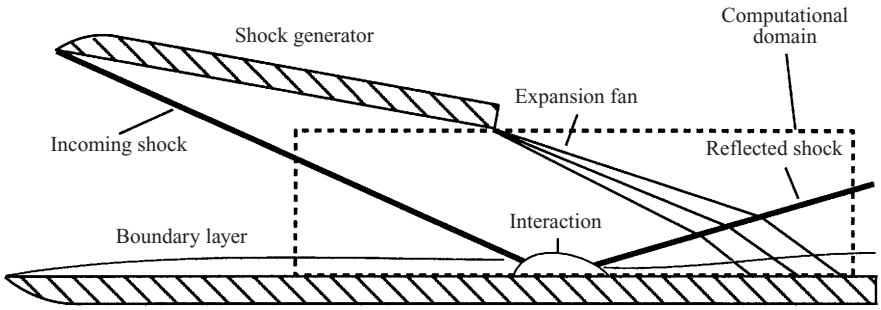

FIGURE 24. Impinging shock at Mach 5. Experimental and computational setup.

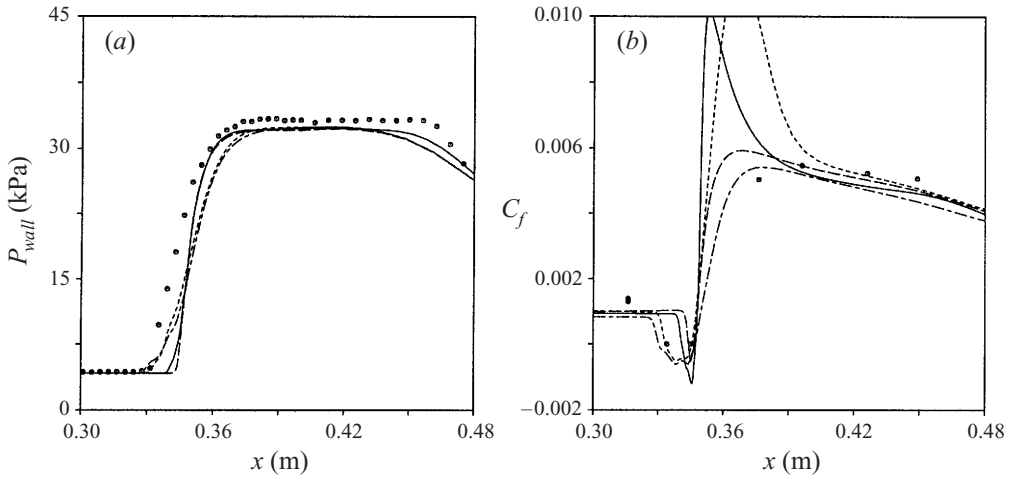

FIGURE 25. (*a*) Wall pressure and (*b*) skin friction coefficient for the impinging shock at Mach 5 with the flow deflection angle $\beta = 10°$. Comparison of the predictions using Chien K–ε (——), Wilcox K–ω (– – –) and the current EARSM based on K–ε (·····) and K–ω (–·–·) with the experiment by Schülein *et al.* (1996) (•).

given by

$$\boldsymbol{a} = \beta_1 \boldsymbol{S}^{2D} + \beta_4 \left(\boldsymbol{S}^{2D}\boldsymbol{\Omega} - \boldsymbol{\Omega}\boldsymbol{S}^{2D} \right) + \beta_a \mathscr{D} \left(\boldsymbol{I}^{2D} - \tfrac{2}{3}\boldsymbol{I} \right) + O(\mathscr{D}^2) \tag{4.10}$$

with β_a from (4.8).

4.2. *Shock/boundary layer interaction*

The compressible form of the proposed model together with the near-wall formulations has been tested on a shock/boundary layer interaction. A turbulent boundary layer at Mach 5 on a flat plate interacts with an oblique shock from a shock generator above the plate, see figure 24. The flow deflection angle is 10° which gives a strong enough shock to cause a boundary layer separation. The experiment by Schülein, Krogmann & Stanewsky (1996) was performed at DLR in Göttingen. Figure 25 shows the computed wall pressure and skin friction coefficient along the flat plate compared to the experimental data. The turbulence models used are the Chien (1982) K–ε model and the Wilcox (1994) K–ω model based on the original eddy-viscosity assumption and also based on the proposed EARSM. The computational results were obtained using the EURANUS code by Rizzi *et al.* (1993). The grid convergence was assessed by repeating the computation on a coarser grid.

The size of the separated region is underestimated by the two eddy-viscosity models whereas a correct separation length is obtained when the models are based on the proposed EARSM. This can be seen both in the skin friction behaviour and in the wall pressure distribution. The computed wall pressure is, however, somewhat shifted downstream.

The Chien K–ε model strongly over-predicts the skin friction downstream of the reattachment point, which is typical for many low Reynolds number K–ε models. This behaviour is inherited by the proposed EARSM based on the Chien K–ε model. The K–ω models give much better skin friction predictions.

5. Diffusion term

In regions of the flow where the production to dissipation ratio is small, the assumption of negligible effects of advection and diffusion of the anisotropy may cause problems, also noticed by Taulbee (1992). In the outer-most part of a boundary layer and in the centre of a turbulent channel flow the magnitude of the β_1-coefficient may thus be too large leading to an overestimation of the $\overline{uv}$ Reynolds stress. The behaviour of the model can be analysed by looking at the effective $C_\mu^{\text{eff}} \equiv -\beta_1/2$ when the strain rate goes to zero, which for the simplified ARSM reads

$$C_\mu^{\text{eff}}(\sigma \to 0) = \frac{3}{5c_1'}. \tag{5.1}$$

For the proposed model constants $C_\mu^{\text{eff}} \approx 0.33$ which is far too high.

In this section we will discuss the possibility of including a correction to the ARSM equations formulated so that the proposed EARSM solution process can be retained. The transport equation for the Reynolds stress anisotropy is given by (1.1) where T_{ijl} and $T_l^{(K)}$ are the flux terms for the Reynolds stress tensor and turbulent kinetic energy. A simple model for the neglected diffusion term may be written as

$$\frac{\partial T_{ijl}}{\partial x_l} - \frac{\overline{u_i u_j}}{K}\frac{\partial T_l^{(K)}}{\partial x_l} = C_D a_{ij}\frac{\partial T_l^{(K)}}{\partial x_l}, \tag{5.2}$$

which gives a modification of the c_1' coefficient in the simplified ARSM equation (2.2). The modified coefficient reads

$$c_1' = \frac{9}{4}\left(c_1 - 1 - \frac{C_D}{\varepsilon}\frac{\partial T_l^{(K)}}{\partial x_l}\right). \tag{5.3}$$

There are, however, numerical problems associated with this form due to the inclusion of the second derivative of K. This could be avoided if the term that balances the turbulent flux term in the K-equation (1.15) is used to approximate the turbulent flux of K:

$$\frac{\partial T_l^{(K)}}{\partial x_l} \approx \mathscr{P} - \varepsilon. \tag{5.4}$$

The advection of K is neglected here. Moreover, the extra term worsens the model behaviour for large strain rates and can even lead to a singular behaviour. The correction thus needs to be switched off for $\mathscr{P}/\varepsilon > 1$. The definition of the c_1' coefficient then becomes

$$c_1' = \frac{9}{4}\left[c_1 - 1 + C_D \max\left(1 - \frac{\mathscr{P}}{\varepsilon}, 0\right)\right]. \tag{5.5}$$

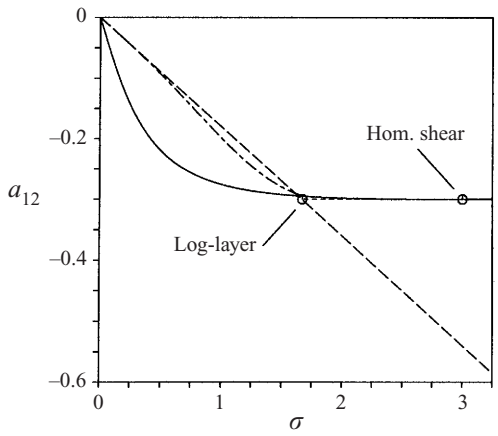

FIGURE 26. The a_{12} anisotropy versus strain rate σ for parallel flow. The current model without (——) and with (–·–·) diffusion model compared to an eddy-viscosity model (– – –) and the Menter (1993) SST model (·····).

The problem with this form is that it is implicit in the $\mathscr{P}/\varepsilon$ ratio and that the max function makes it impossible to solve. The diffusion model will thus be further approximated by using $\mathscr{P}/\varepsilon = -\beta_1 II_S$. If β_1 is approximated with β_1^{eq} where $\mathscr{P} = \varepsilon$, the correction is guaranteed to be zero in the log-layer and for higher strain rates. The definition of the c_1' coefficient now becomes

$$c_1' = \tfrac{9}{4}\left[c_1 - 1 + C_D \max\left(1 + \beta_1^{\text{eq}} II_S, 0\right)\right] \tag{5.6}$$

where

$$\beta_1^{\text{eq}} = -\frac{6}{5}\frac{N^{\text{eq}}}{(N^{\text{eq}})^2 - 2II_\Omega} \tag{5.7}$$

and

$$N^{\text{eq}} = \tfrac{9}{4}c_1. \tag{5.8}$$

The constant C_D can now be estimated by looking at the effective C_μ for zero strain rates in (5.1). With $C_D = 2.2$ the effective C_μ becomes $C_\mu^{\text{eff}} = 0.09$ which is close to what one should expect. The a_{12} anisotropy with the proposed diffusion model is compared to the basic EARSM in figure 26 for parallel flow (cf. figure 4). The inclusion of the diffusion model makes the proposed EARSM behave almost the same as the SST model for this case. In figure 27 we can see an improvement of the a_{12} anisotropy prediction near the centre of the channel simulated by Kim (1989). The actual difference in the predicted mean velocity profile is quite small. This improvement is similar in character to that obtained by the correction introduced by Taulbee (1992) although the two approaches are motivated differently.

The derivation of the diffusion correction is based on a number of *ad hoc* arguments and should be seen only as a possible extension of the model to flow situations where diffusion may be of substantial importance.

6. Concluding remarks

For two-dimensional mean flows the new proposed EARSM represents an exact solution of the implicit ARSM relation for the anisotropy tensor, but also a good approximation for three-dimensional mean flows. The fact that it fully accounts for

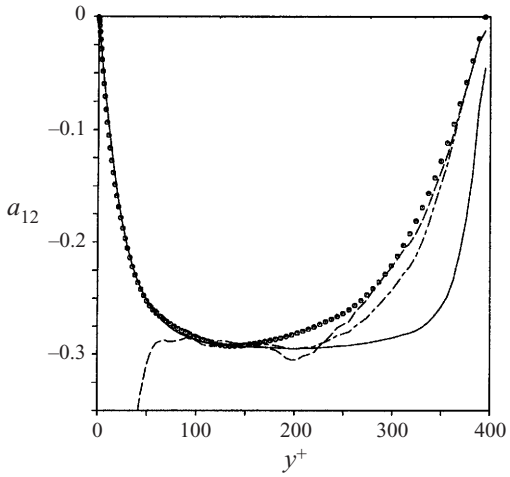

FIGURE 27. The a_{12} anisotropy in channel flow. Comparison of the current EARSM without (——) and with (–·–·) diffusion model with the eddy-viscosity model (– – –) and DNS data (•) (Kim 1989).

three-dimensional effects gives it a natural predictive capability for complex flows. This was demonstrated here by capturing the correct trends for axially rotating pipe flow. Standard two-equation models predict a solid-body rotation with an unaffected axial velocity profile. In reality the azimuthal velocity has a variation that is close to parabolic and the rotation causes the axial velocity profile to be less full, i.e. more parabolic. To capture these features the model description of the inter-component transfer is crucial. For instance, the simplified linear rapid pressure–strain model of Launder *et al.* (1975) and Naot, Shavit & Wolfstein (1973), usually referred to as the isotropization of production model, does not have the necessary ingredients. The full linear model, on the other hand, together with linear models for the other terms, was demonstrated here to be sufficient to capture the main features of the flow in the axially rotating pipe. In general the predictive capability of the proposed EARSM for rotating flows is substantially better than standard two-equation models and than EARSM formulations including only terms up to second order in $\boldsymbol{S}$ and $\boldsymbol{\Omega}$.

The extension to compressible flows is done in a simple way in the present EARSM in which the equations are expressed by use of Favre averages. Compressibility of the mean flow is accounted for, but no explicit compressibility corrections are added to the 'platform' (K–ε, K–ω …) equations. With some minor redefinitions the same ARSM relation for a_{ij} as for incompressible flow could be used also here. This approach for wall-bounded turbulent flows is adequate for Mach numbers up to about 5. It was shown to capture the essential features of the complex interaction between an inclined shock and a turbulent boundary layer at Mach 5. In particular it describes the skin friction and separation length much better than standard two-equation models. Compared to the standard two-equation models on which the present EARSM is based it also gives a substantial improvement for the prediction of the skin friction variation in incompressible boundary layers with adverse pressure gradient (detailed results not reported here).

Poor prediction of the effects of rotation and the under-prediction of separation tendency in adverse pressure gradient boundary layers are well known deficiencies of closures based on the eddy-viscosity hypothesis. The present EARSM substantially improves these two aspects, and reduces the need for wall damping. A simple way

to obtain the correct near-wall limits of the anisotropies was constructed here on the basis of a van Driest type of damping function. For channel flow this was shown to give a very accurate description, and a simple method to retain numerical stability for situations with separated flows was demonstrated. A form of wall damping function based on $Re_y \equiv \sqrt{K}y/\nu$ was shown to be an attractive alternative to forms based on y^+ in flows with (or near) separation.

The reduced need for wall damping is coupled to the fact that the present EARSM automatically predicts a production to dissipation ratio with correct asymptotic behaviour for large strain rates. For instance, in parallel flows this correctly gives an asymptotically constant shear stress anisotropy component for large strains (shear rates). This behaviour is not a natural part of eddy-viscosity based models, but was incorporated in a somewhat *ad hoc* manner by Menter (1993). In the present model this behaviour emanates naturally from the underlying modelling of the terms in the RST equations and the direct solution of the production to dissipation ratio.

To further illustrate the behaviour for large strain rates the proposed model was tested in homogeneous shear flow at high initial shear rate. The good prediction that was obtained for this case can, however, be regarded as a bit fortuitous in the light of the fact that the basic ARSM approximation is somewhat questionable for a case with a significantly non-zero left-hand side of the a_{ij} transport equation ($\partial a_{ij}/\partial t \neq 0$). Moreover, the Launder *et al.* (1975) model does not give accurate predictions of this case when used in a differential form. It is, however, a fact that the self-consistent approach (i.e. where the production to dissipation ratio is solved for as part of the total EARSM-solution) gives a model with the correct asymptotic behaviour, which is a pre-requisite for reasonable predictions in the limit of high shear. The present model is not constructed specifically to incorporate such effects. It is, however, an important step towards a more general engineering model that the model is also able to give reasonable results in extreme flow cases.

Perhaps the most important feature of the proposed model is the numerical behaviour. The computational cost is not significantly increased compared to standard eddy-viscosity two-equation models and the general numerical behaviour is almost the same. Implementation of this model into flow solvers with existing eddy-viscosity two-equation models should not pose major problems. The model may be formulated in terms of an effective eddy viscosity with an additional correction that may be treated fully explicitly (see Appendix A).

The authors would like to thank Dr Torbjörn Sjögren and Dr Magnus Hallbäck for many helpful discussions, especially concerning the treatment of rotating coordinate systems. The first author would also like to thank Dr Sharath Girimaji for many helpful discussions, especially concerning non-equilibrium turbulence. The authors gratefully acknowledge funding of this study from the European Space Agency within a project for improving the modelling of turbulent flows related to hypersonic lifting vehicles and would like to acknowledge Dr Ingemar Lindblad for leading this project.

Appendix A. Summary of the proposed model

The Reynolds stresses may be written in terms of an effective C_μ-coefficient which is mathematically identical with the formulation in § 2:

$$\overline{u_i u_j} = K(\tfrac{2}{3}\delta_{ij} - 2C_\mu^{\text{eff}} S_{ij} + a_{ij}^{(\text{ex})}), \tag{A 1}$$

where the effective C_μ-coefficient is

$$C_\mu^{\text{eff}} = -\tfrac{1}{2} f_1 \left(\beta_1 + II_\Omega \beta_6\right), \tag{A 2}$$

and the extra anisotropy $a_{ij}^{(\text{ex})}$ then becomes

$$\begin{aligned} \boldsymbol{a}^{(\text{ex})} = {} & \left(1 - f_1^2\right) \frac{3B_2 - 4}{\max\left(II_S, II_S^{\text{eq}}\right)} + f_1^2 \beta_3 \left(\boldsymbol{\Omega}^2 - \tfrac{1}{3} II_\Omega \, \boldsymbol{I}\right) \left(\boldsymbol{S}^2 - \tfrac{1}{3} II_S \, \boldsymbol{I}\right) \\ & + \left(f_1^2 \beta_4 - \left(1 - f_1^2\right) \frac{B_2}{2\max\left(II_S, II_S^{\text{eq}}\right)} \right) (\boldsymbol{S\Omega} - \boldsymbol{\Omega S}) \\ & + f_1 \beta_6 \left(\boldsymbol{S\Omega}^2 + \boldsymbol{\Omega}^2 \boldsymbol{S} - II_\Omega \boldsymbol{S} - \tfrac{2}{3} IV \, \boldsymbol{I}\right) + f_1^2 \beta_9 \left(\boldsymbol{\Omega S \Omega}^2 - \boldsymbol{\Omega}^2 \boldsymbol{S \Omega}\right). \end{aligned} \tag{A 3}$$

Here $\boldsymbol{a}$, $\boldsymbol{S}$ and $\boldsymbol{\Omega}$ denote second rank tensors, $\text{tr}\{\ \}$ denotes the trace and $\boldsymbol{I}$ is the identity matrix. The inner product of two matrices is defined as $(\boldsymbol{SS})_{ij} \equiv \left(\boldsymbol{S}^2\right)_{ij} \equiv S_{ik} S_{kj}$. The normalized mean strain and rotation tensors are defined as

$$S_{ij} = \frac{\tau}{2} \left(U_{i,j} + U_{j,i}\right), \quad \Omega_{ij} = \frac{\tau}{2} \left(U_{i,j} - U_{j,i}\right), \tag{A 4}$$

where the turbulent timescale is defined by

$$\tau = \max\left(\frac{K}{\varepsilon}, C_\tau \sqrt{\frac{\nu}{\varepsilon}}\right). \tag{A 5}$$

The invariants are defined by

$$II_S = \text{tr}\{\boldsymbol{S}^2\}, \quad II_\Omega = \text{tr}\{\boldsymbol{\Omega}^2\}, \quad IV = \text{tr}\{\boldsymbol{S\Omega}^2\}, \quad V = \text{tr}\{\boldsymbol{S}^2 \boldsymbol{\Omega}^2\}, \tag{A 6}$$

and

$$II_S^{\text{eq}} = \frac{405 c_1^2}{216 c_1 - 160}. \tag{A 7}$$

By introducing an effective C_μ-coefficient one can easily introduce this level of modelling into flow solvers with existing two-equation eddy-viscosity models by setting

$$\nu_t = C_\mu^{\text{eff}} K \tau. \tag{A 8}$$

The contribution from the extra anisotropy $a_{ij}^{(\text{ex})}$ may now be added as fully explicit additional terms in the equations.

The β-coefficients are given by

$$\left.\begin{aligned} \beta_1 &= -\frac{N\left(2N^2 - 7II_\Omega\right)}{Q}, & \beta_3 &= -\frac{12 N^{-1} IV}{Q}, & \\ \beta_4 &= -\frac{2\left(N^2 - 2II_\Omega\right)}{Q}, & \beta_6 &= -\frac{6N}{Q}, & \beta_9 &= \frac{6}{Q}, \end{aligned}\right\} \tag{A 9}$$

with the denominator

$$Q = \tfrac{5}{6} \left(N^2 - 2II_\Omega\right) \left(2N^2 - II_\Omega\right). \tag{A 10}$$

For most purposes it is sufficient to take $N = N_c$ where

$$N_c = \begin{cases} \frac{c_1'}{3} + (P_1 + \sqrt{P_2})^{1/3} + \mathrm{sign}\,(P_1 - \sqrt{P_2}) \mid P_1 - \sqrt{P_2} \mid^{1/3}, & P_2 \geqslant 0 \\ \frac{c_1'}{3} + 2\left(P_1^2 - P_2\right)^{1/6} \cos\left(\frac{1}{3}\arccos\left(\frac{P_1}{\sqrt{P_1^2 - P_2}}\right)\right), & P_2 < 0, \end{cases} \tag{A 11}$$

with

$$P_1 = \left(\frac{c_1'^2}{27} + \frac{9}{20}II_S - \frac{2}{3}II_\Omega\right)c_1', \quad P_2 = P_1^2 - \left(\frac{c_1'^2}{9} + \frac{9}{10}II_S + \frac{2}{3}II_\Omega\right)^3 \tag{A 12}$$

and

$$c_1' = \tfrac{9}{4}(c_1 - 1). \tag{A 13}$$

An additional term can be added to N_c in order to improve the accuracy for three-dimensional mean flows (see § 2.2).

The simplifications for two-dimensional mean flow are

$$\beta_1 = -\frac{6}{5}\frac{N_c}{N_c^2 - 2II_\Omega}, \quad \beta_4 = -\frac{6}{5}\frac{1}{N_c^2 - 2II_\Omega}, \quad \beta_3 = \beta_6 = \beta_9 = 0. \tag{A 14}$$

The damping function reads

$$f_1 = 1 - \exp\left(-C_{y1}'\sqrt{Re_y} - C_{y2}'Re_y^2\right), \tag{A 15}$$

where

$$Re_y = \frac{\sqrt{K}\,y}{\nu}. \tag{A 16}$$

Finally, the five model constants are

$$C_\tau = 6.0, \quad c_1 = 1.8, \quad B_2 = 1.8, \quad C_{y1}' = \frac{2.4}{26.0}, \quad C_{y2}' = \frac{0.003}{26.0}. \tag{A 17}$$

Appendix B. The completeness of the $\boldsymbol{a}(\boldsymbol{S}, \boldsymbol{\Omega})$ expression with ten terms

Based on the derivations of Spencer & Rivlin (1959) for matrix polynomials Pope (1975) concluded that there are ten independent terms in the complete expression $\boldsymbol{a}(\boldsymbol{S}, \boldsymbol{\Omega})$. One should here restrict the meaning of independence to polynomial independence as was also pointed out by Taulbee, Sonnenmeier & Wall (1994). The highest-order term $\left(\boldsymbol{\Omega S}^2\boldsymbol{\Omega}^2 - \boldsymbol{\Omega}^2\boldsymbol{S}^2\boldsymbol{\Omega}\right)$ in expression (1.18) is of order 5 and extension 3.

The $\boldsymbol{S}$ and $\boldsymbol{\Omega}$ tensors can appear in powers up to 2. A term $\boldsymbol{S}^m\boldsymbol{\Omega}^n$ is then said to be of power $m + n$ and extension 2, etc. Shih & Lumley (1993) (see also Shih 1996) also include a term of power 6 and extension 4. They use a notation with the mean velocity gradient tensor and its transpose, but with the present notation such a term can be written as

$$\boldsymbol{S\Omega}^2\boldsymbol{S}^2\boldsymbol{\Omega} - \boldsymbol{\Omega S}^2\boldsymbol{\Omega}^2\boldsymbol{S} - \tfrac{2}{3}VI\ \boldsymbol{I}, \tag{B 1}$$

where the invariant VI equals $\mathrm{tr}\{\boldsymbol{S\Omega}^2\boldsymbol{S}^2\boldsymbol{\Omega}\}$. One may first note that the invariant VI is of third power in $\boldsymbol{\Omega}$, which means that it cannot be expressed in terms of a polynomial in the other invariants, which are of order zero or two in $\boldsymbol{\Omega}$. Hence, VI contains sign information that is not contained in the other invariants. We can derive

the following relation for its square:

$$VI^2 = \frac{II_\Omega^3}{144}\left(9{II_S}^3 + 2III_S^2\right) + \frac{II_\Omega^2}{6}\left(-3VII_S^2 + IV\,II_S\,III_S\right)$$
$$+\frac{II_\Omega}{8}\left(10\,V^2II_S - 4VIV\,III_S - IV^2II_S^2\right) - V^3 + \tfrac{1}{2}VIV^2II_S - \tfrac{1}{3}IV^3III_S.$$

In the present modelling the invariant VI will not appear since it would arise from the product of the highest (fifth-order) term and $\boldsymbol{S}$, and even in the general solution (for $c_2 \neq \frac{5}{9}$) the coefficient $\beta_{10} = 0$.

We can furthermore express the sixth-order term as the following combination of lower-order terms:

$$\boldsymbol{S\Omega}^2\boldsymbol{S}^2\boldsymbol{\Omega} - \boldsymbol{\Omega S}^2\boldsymbol{\Omega}^2\boldsymbol{S} - \tfrac{2}{3}VI\ \boldsymbol{I} = \left(\tfrac{2}{3}V + \tfrac{1}{12}II_SII_\Omega\right)(\boldsymbol{S\Omega} - \boldsymbol{\Omega S})$$
$$+\tfrac{1}{3}IV\left(\boldsymbol{S}^2\boldsymbol{\Omega} - \boldsymbol{\Omega S}^2\right) - \tfrac{1}{6}II_\Omega\left(\boldsymbol{S\Omega S}^2 - \boldsymbol{S}^2\boldsymbol{\Omega S}\right) + \tfrac{1}{6}II_S\left(\boldsymbol{\Omega S\Omega}^2 - \boldsymbol{\Omega}^2\boldsymbol{S\Omega}\right).$$

By use of the generalized Cayley–Hamilton theorem it is fairly straightforward to show that no other independent sixth- or higher-order term exists (see e.g. Shih & Lumley (1993).

Appendix C. Solution of the general quasi-linear ARSM equation

The implicit general quasi-linear ARSM equation is rewritten similarly to the simplified equation (2.2)

$$N\boldsymbol{a} = -A_1\boldsymbol{S} + (\boldsymbol{a\Omega} - \boldsymbol{\Omega a}) - A_2\left(\boldsymbol{aS} + \boldsymbol{Sa} - \tfrac{2}{3}\mathrm{tr}\{\boldsymbol{aS}\}\right), \tag{C 1}$$

where

$$N = A_3 + A_4\frac{\mathscr{P}}{\varepsilon}. \tag{C 2}$$

The simplified equation is now a special case of (C 1) with the coefficients $A_1 = \frac{6}{5}$, $A_2 = 0$, $A_3 = c_1'$ and $A_4 = \frac{9}{4}$. For the general case we require that A_1, A_3 and A_4 are positive.

C.1. *Solution for two-dimensional mean flow*

The solution for two-dimensional mean flow is

$$\beta_1 = -\frac{A_1N}{Q}, \quad \beta_2 = 2\frac{A_1A_2}{Q}, \quad \beta_4 = -\frac{A_1}{Q}, \tag{C 3}$$

where the denominator

$$Q = N^2 - 2II_\Omega - \tfrac{2}{3}A_2^2II_S. \tag{C 4}$$

The equation for N is, for two-dimensional mean flow,

$$N^3 - A_3N^2 - \left(\left(A_1A_4 + \tfrac{2}{3}A_2^2\right)II_S + 2II_\Omega\right)N + 2A_3\left(\tfrac{1}{3}A_2^2II_S + II_\Omega\right) = 0, \tag{C 5}$$

with the solution

$$N = \begin{cases} \dfrac{A_3}{3} + (P_1 + \sqrt{P_2})^{1/3} + \mathrm{sign}\,(P_1 - \sqrt{P_2})\mid P_1 - \sqrt{P_2}\mid^{1/3}, & P_2 \geqslant 0 \\ \dfrac{A_3}{3} + 2(P_1^2 - P_2)^{1/6}\cos\left(\dfrac{1}{3}\arccos\left(\dfrac{P_1}{\sqrt{P_1^2 - P_2}}\right)\right), & P_2 < 0, \end{cases} \tag{C 6}$$

where

$$P_1 = \left(\frac{A_3^2}{27} + \left(\frac{A_1 A_4}{6} - \tfrac{2}{9}A_2^2\right) II_S - \tfrac{2}{3} II_\Omega\right) A_3 \tag{C 7}$$

and

$$P_2 = P_1^2 - \left(\frac{A_3^2}{9} + \left(\frac{A_1 A_4}{3} + \tfrac{2}{9}A_2^2\right) II_S + \tfrac{2}{3} II_\Omega\right)^3. \tag{C 8}$$

Let us investigate whether the denominator in equation (C 4) can become zero. Equation (C 5) can be rewritten, by using equation (C 4), as

$$Q\,(N - A_3) = A_1 A_4 II_S N, \tag{C 9}$$

which shows that $Q > 0$ if $N > A_3$. The problem is then to show that $N > A_3$. Let us first look at the special case when $II_S = 0$. Equation (C 5) can then be written

$$(N - A_3)\left(N^2 - 2II_\Omega\right) = 0, \tag{C 10}$$

with the only real root $N = A_3$. Differentiating equation (C 5) with respect to II_S gives

$$\frac{\partial N}{\partial II_S} = \frac{\tfrac{2}{3}A_2^2\,(N - A_3) + A_1 A_4 N}{3\left(N - \tfrac{2}{3}A_3\right) N - \left(A_1 A_4 + \tfrac{2}{3}A_2^2\right) II_S - 2II_\Omega}, \tag{C 11}$$

which is positive if $N \geqslant A_3$. When $II_S = 0$ (C 11) can be written as

$$\left.\frac{\partial N}{\partial II_S}\right|_{II_S = 0} = \frac{A_1 A_3 A_4}{A_3^2 - 2II_\Omega} > 0. \tag{C 12}$$

So far we know that $N = A_3$ for $II_S = 0$ and that N increases until (C 11) changes sign. By using (C 5) II_Ω can be eliminated in (C 11) which then becomes

$$\frac{\partial N}{\partial II_S} = \frac{\tfrac{2}{3}A_2^2\,(N - A_3)^2 + A_1 A_4 N\,(N - A_3)}{2N\,(N - A_3)^2 + A_1 A_3 A_4 II_S}. \tag{C 13}$$

From this form it is obvious that the denominator is strictly positive and that $\partial N/\partial II_S = 0$ for $II_S = 0$ only (where $N = A_3$). Hence, the numerator is strictly positive and N increases for all II_S, showing that $N \geqslant A_3$ for all II_S. The corresponding relation for the simplified ARSM equation is $N \geqslant c_1'$.

The denominator Q is thus always positive which guarantees a non-singular solution.

C.2. *Solution for three-dimensional mean flow*

The solution of the linear equation system where N is assumed as known can be formulated as (see Gatski & Speziale 1993)

$$N\beta_\lambda = -A_1\delta_{1\lambda} + \sum_\gamma J_{\lambda\gamma}\beta_\gamma - A_2 \sum_\gamma H_{\lambda\gamma}\beta_\gamma \tag{C 14}$$

or in the standard form for linear equation systems

$$\left(N\delta_{\gamma\lambda} - J_{\gamma\lambda} + A_2 H_{\gamma\lambda}\right)\beta_\lambda = -A_1\delta_{1\gamma} \tag{C 15}$$

where the matrices are given below for three-dimensional mean flow

$$\boldsymbol{H} = \begin{bmatrix}
0 & \frac{1}{3}II_S & -\frac{2}{3}II_\Omega & 0 & 0 & \frac{2}{3}IV & -\frac{1}{3}V & 0 & 0 & 0 \\
2 & 0 & 0 & 0 & 0 & 2II_\Omega & IV & 0 & 0 & 0 \\
0 & 0 & 0 & 0 & 0 & II_S & \frac{1}{3}III_S & 0 & 0 & 0 \\
0 & 0 & 0 & 0 & \frac{1}{2}II_S & 0 & 0 & \frac{1}{3}III_S & -IV & -\frac{1}{3}V - \frac{1}{6}II_S II_\Omega \\
0 & 0 & 0 & 1 & 0 & 0 & 0 & 0 & -II_\Omega & -\frac{2}{3}IV \\
0 & 0 & 1 & 0 & 0 & 0 & \frac{1}{2}II_S & 0 & 0 & 0 \\
0 & 0 & 0 & 0 & 0 & -1 & 0 & 0 & 0 & 0 \\
0 & 0 & 0 & 0 & -1 & 0 & 0 & 0 & 0 & \frac{1}{3}II_\Omega \\
0 & 0 & 0 & 0 & 0 & 0 & 0 & 0 & 0 & -\frac{1}{3}II_S \\
0 & 0 & 0 & 0 & 0 & 0 & 0 & 0 & -2 & 0
\end{bmatrix}, \tag{C 16}$$

$$\boldsymbol{J} = \begin{bmatrix}
0 & 0 & 0 & -II_\Omega & 0 & 0 & 0 & 2V - II_S II_\Omega & II_\Omega^2 & 0 \\
0 & 0 & 0 & 0 & -II_\Omega & 0 & 0 & -2IV & 0 & II_\Omega^2 \\
0 & 0 & 0 & 0 & -2II_S & 0 & 0 & 0 & -2IV & 2II_S II_\Omega - 2V \\
1 & 0 & 0 & 0 & 0 & \frac{1}{2}II_\Omega & 0 & 0 & 0 & 0 \\
0 & 1 & 0 & 0 & 0 & 0 & \frac{1}{2}II_\Omega & 0 & 0 & 0 \\
0 & 0 & 0 & 3 & 0 & 0 & 0 & II_S & -2II_\Omega & 0 \\
0 & 0 & 0 & 0 & 3 & 0 & 0 & 0 & 0 & -2II_\Omega \\
0 & 0 & 0 & 0 & 0 & 0 & 0 & 0 & 0 & 0 \\
0 & 0 & 0 & 0 & 0 & -1 & 0 & 0 & 0 & 0 \\
0 & 0 & 0 & 0 & 0 & 0 & -1 & 0 & 0 & 0
\end{bmatrix}. \tag{C 17}$$

The solution for three-dimensional mean flow is

$$\left.\begin{aligned}
\beta_1 &= -\tfrac{1}{2}A_1 N\left(30A_2 IV - 21N II_\Omega - 2A_2^3 III_S + 6N^3 - 3A_2^2 II_S N\right)/Q, \\
\beta_2 &= -A_1 A_2\left(6A_2 IV + 12N II_\Omega + 2A_2^3 III_S - 6N^3 + 3A_2^2 II_S N\right)/Q, \\
\beta_3 &= -3A_1\left(2A_2^2 III_S + 3NA_2 II_S + 6IV\right)/Q, \\
\beta_4 &= -A_1\left(2A_2^3 III_S + 3A_2^2 N II_S + 6A_2 IV - 6N II_\Omega + 3N^3\right)/Q, \\
\beta_5 &= 9A_1 A_2 N^2/Q, \quad \beta_6 = -9A_1 N^2/Q, \quad \beta_7 = 18A_1 A_2 N/Q, \\
\beta_8 &= 9A_1 A_2^2 N/Q, \quad \beta_9 = 9A_1 N/Q, \quad \beta_{10} = 0,
\end{aligned}\right\} \tag{C 18}$$

with the denominator

$$\begin{aligned}
Q = {} & 3N^5 + \left(-\tfrac{15}{2}II_\Omega - \tfrac{7}{2}A_2^2 II_S\right)N^3 + \left(21A_2 IV - A_2^3 III_S\right)N^2 \\
& + \left(3II_\Omega^2 - 8II_S II_\Omega A_2^2 + 24A_2^2 V + A_2^4 II_S^2\right)N + \tfrac{2}{3}A_2^5 II_S III_S
\end{aligned}$$

$$+2A_2^3\,IV\,II_S - 2A_2^3\,II_\Omega\,III_S - 6\,IV\,A_2\,II_\Omega. \qquad \text{(C 19)}$$

By substituting $N = 1$, $A_1 = 1$ and $A_2 = 1$ one gets the same ARSM equation as Gatski & Speziale (1993) and also an identical solution.

The equation for N can also be derived for three-dimensional mean flow and is a sixth- order polynomial equation, as for the simplified case. The expression is, however, complicated and of small practical interest. As for the solution of the simplified ARSM equation, the two-dimensional solution of N can also be used here as a first approximation.

REFERENCES

Chien, K. Y. 1982 Predictions of channel and boundary-layer flows with a low-Reynolds-number turbulence model. *AIAA J.* **20**, 33–38.

Cook, P. H., MacDonald, M. A. & Firmin, M. C. P. 1979 Aerofoil 2822 – Pressure distributions, boundary layer and wake measurements. *AGARD AR* 138.

Daly, B. J. & Harlow, F. H. 1970 Transport equations in turbulence. *Phys. Fluids* **13**, 2634–2649.

Durbin, P. A. 1993 Application of a near-wall turbulence model to boundary layers and heat transfer. *Intl J. Heat Fluid Flow* **14**, 316–323.

Durbin, P. A. 1995 Separated flow computations with the k–ε–v^2 model. *AIAA J.* **33**, 659–664.

Friedrich, R. & Bertolotti, F. P. 1997 Compressibility effects due to turbulent fluctuations. *Appl. Sci. Res.* **57**, 165–194.

Gatski, T. B & Speziale C. G. 1993 On explicit algebraic stress models for complex turbulent flows. *J. Fluid Mech.* **254**, 59–78.

Girimaji, S. S. 1996*a* Fully-explicit and self-consistent algebraic Reynolds stress model. *Theor. and Comp. Fluid Dyn.* **8**, 387–402 (also *ICASE Rep.* 95-82).

Girimaji, S. S. 1996*b* Improved algebraic Reynolds stress model for engineering flows. In *Engineering Turbulence Modelling and Experiments 3* (ed. W. Rodi & G. Bergeles), pp. 121–129. Elsevier.

Girimaji, S. S. 1997 A Galilean invariant explicit algebraic Reynolds stress model for turbulent curved flows. *Phys. Fluids* **9**, 1067–1077 (also *ICASE Rep.* 96-38).

Hanjalić, K., Jakirlić, S. & Hadžić, I. 1995 Computation of oscillating turbulent flows at transitional *Re*-numbers. In *Turbulent Shear Flows 9* (ed. F. Durst, N. Kasagi & B. E. Launder), pp. 323–342. Springer.

Hellström, T., Davidson, L. & Rizzi, A. 1994 Reynolds stress transport modelling of transonic flow around the RAE2822 airfoil. *AIAA Paper* 94-0309.

Horsten, J. J., Boer, R. G. den & Zwaan, R. J. 1983 Unsteady transonic pressure measurements on a semi-span wind tunnel model of a transport-type supercritical wing (LANN model). *AFWAL-TR*-83-3039.

Imao, S., Itoh, M. & Harada, T. 1996 Turbulent characteristics of the flow in an axially rotating pipe. *J. Heat Fluid Flow* **17**, 444–451.

Johansson, A. V. & Wallin, S. 1996 A new explicit algebraic Reynolds stress model. *Proc. Sixth European Turbulence Conference, Lausanne, July 1996* (ed. S. Gavrilakis, L. Machiels & P. A. Monkewitz), pp. 31–34. Kluwer.

Kim, J. 1989 On the structure of pressure fluctuations in simulated turbulent channel flow. *J. Fluid Mech.* **205**, 421–451.

Launder, B. E., Reece, G. J. & Rodi, W. 1975 Progress in the development of a Reynolds-stress turbulence closure. *J. Fluid Mech.* **41**, 537–566.

Lumley, J. L. 1978 Computational modeling of turbulent flows. *Adv. Appl. Mech.* **18**, 123–176.

Matsson, O. J. E. & Alfredsson, P. H. 1990 Curvature- and rotation-induced instabilities in channel flow. *J. Fluid Mech.* **210**, 537–563.

Menter, F. R. 1993 Zonal two equation k–ω turbulence models for aerodynamic flows. *AIAA Paper* 93-2906.

Menter, F. R. 1994 Two-equation eddy-viscosity turbulence models for engineering applications. *AIAA J.* **32**, 1598–1604.

Moser, R. D, Kim J. & Mansour N. N. 1998 DNS of turbulent channel flow up to $Re_\tau = 590$. *Phys. Fluids* **11**, 943–945.

Naot, D., Shavit, A. & Wolfstein, M. 1973 Two-point correlation model and the redistribution of Reynolds stresses. *Phys. Fluids* **16**, 738–743.

Pope, S. B. 1975 A more general effective-viscosity hypothesis. *J. Fluid Mech.* **72**, 331–340.

Rizzi, A., Eliasson, P., Lindblad, I., Hirsch C., Lacor, C. & Haeuser, J. 1993 The engineering of multiblock/multigrid software for Navier–Stokes flows on structured meshes. *Computers Fluids* **22**, 341–367.

Rodi, W. 1972 The prediction of free turbulent boundary layers by use of a two equation model of turbulence. PhD thesis, University of London.

Rodi, W. 1976 A new algebraic relation for calculating the Reynolds stresses. *Z. Angew. Math. Mech.* **56**, T219–221.

Rotta, J.C. 1951 Statistische Theorie nichthomogener Turbulenz. *Z. Phys.* **129**, 547–572.

Schlichting, H. 1979 *Boundary-Layer Theory*, 7th edn. McGraw-Hill.

Schülein, E., Krogmann, P. & Stanewsky, E. 1996 Documentation of two-dimensional impinging shock/turbulent boundary layer interaction flow. *DLR Rep.* DLR IB 223-96 A 49.

Shabbir, A. & Shih, T. H. 1992 Critical assessment of Reynolds stress turbulence models using homogeneous flows. *NASA TM* 105954; *ICOMP*-92-24; *CMOTT*-92-12.

Shih, T.-H. 1996 Constitutive relations and realizability of single-point turbulence closures. In *Turbulence and Transition Modelling* (ed. M. Hallback, D. S. Henningson, A. V. Johansson & P. H. Alfredsson). Kluwer.

Shih, T.-H. & Lumley, J. L. 1993 Remarks on turbulent constitutive relations. *Math. Comput. Modelling*, **18**, 9–16.

Shih, T. H., Zhu, J. & Lumley, J. L. 1992 A realizable Reynolds stress algebraic equation model. *NASA TM* 105993; *ICOMP*-92-27; *CMOTT*-92-14.

Shih, T.-H., Zhu, J. & Lumley, J. L. 1995 A new Reynolds stress alegebraic equation model. *Comput. Meth. Appl. Mech. Engng* **125**, 287–302.

Sjögren, T. 1997 Development and validation of turbulence models through experiment and computation. Doctoral thesis, Dept. of Mechanics, KTH, Stockholm, Sweden.

So, R. M. C., Lai, Y. G. & Zhang, H. S. 1991 Second-order near-wall turbulence closures: a review. *AIAA J.* **29**, 1819–1835.

Spalart, P. R. 1988 Direct simulation of a turbulent boundary layer up to $R_\theta = 1410$. *J. Fluid Mech.* **187**, 61–98.

Spencer, A. J. M. & Rivlin, R. S. 1959 The theory of matrix polynomials and its application to the mechanics of isotropic continual. *Arch. Rat. Mech. Anal.* **2**, 309–336.

Speziale, C. G., Sarkar, S. & Gatski, T. B. 1991 Modelling the pressure–strain correlation of turbulence: an invariant dynamical systems approach. *J. Fluid Mech.* **227**, 245–272.

Speziale, C. G. & Xu, X.-H. 1996 Towards the development of second-order closure models for nonequilibrium turbulent flows. *Intl J. Heat Fluid Flow* **17**, 238–244.

Taulbee, D. B. 1992 An improved algebraic Reynolds stress model and corresponding nonlinear stress model. *Phys. Fluids* A **4**, 2555–2561.

Taulbee, D. B., Sonnenmeier, J. R. & Wall, K. M. 1994 Stress relation for three-dimensional turbulent flows. *Phys. Fluids* **6**, 1399–1401.

Tavoularis, S. & Corrsin, S. 1981 Experiments in nearly homogeneous turbulent shear flow with a uniform mean temperature gradient. Part I. *J. Fluid Mech.* **104**, 311–347.

Vandromme, D. 1992 Introduction to the modeling of turbulence. *Von Karman Institute for Fluid Dynamics, Lecture Series* 1991-02.

Wallin, S. & Johansson, A. V. 1996 A new explicit algebraic Reynolds stress turbulence model including an improved near-wall treatment. *Proc. Flow Modeling and Turbulence Measurements VI, Tallahassee F. L.* (ed. C.-J. Chen, C. Shih, J. Lienau & R. J. Kung), pp. 399–406. Balkema.

Wilcox, D. C. 1988 Reassessment of the scale-determining equation for advanced turbulence models. *AIAA J.* **26**, 1299–1310.

Wilcox, D. C. 1993 *Turbulence Modeling for CFD*. DCW Industries Inc., La Cañada, California.

Wilcox, D. C. 1994 Simulation of transition with a two-equation turbulence model. *AIAA J.* **32**, 247–255.